Received October 1998
Revised August 1999
Accepted September 1999

A conservative finite difference method and its application for the analysis of a transient flow around a square prism

A.N. Pavlov
Institute for Mathematical Modelling, Russian Academy of Sciences, Moscow, Russia
S.S. Sazhin
School of Engineering, Faculty of Science and Engineering, University of Brighton, Brighton, UK
R.P. Fedorenko
Keldysh Institute of Applied Mathematics, Russian Academy of Sciences, Moscow, Russia, and
M.R. Heikal
Institute for Mathematical Modelling, Russian Academy of Sciences, Moscow, Russia

Keywords *Transient flow, Energy conservation, Numerical methods*

Abstract *Detailed results of numerical calculations of transient, 2D incompressible flow around and in the wake of a square prism at Re = 100, 200 and 500 are presented. An implicit finite-difference operator-splitting method, a version of the known SIMPLEC-like method on a staggered grid, is described. Appropriate theoretical results are presented. The method has second-order accuracy in space, conserving mass, momentum and kinetic energy. A new modification of the multigrid method is employed to solve the elliptic pressure problem. Calculations are performed on a sequence of spatial grids with up to 401 × 321 grid points, at sequentially halved time steps to ensure grid-independent results. Three types of flow are shown to exist at Re = 500: a steady-state unstable flow and two which are transient, fully periodic and asymmetric about the centre line but mirror symmetric to each other. Discrete frequency spectra of drag and lift coefficients are presented.*

1. Introduction

In most practical applications of computational fluid dynamics (CFD) attention is focused on finding a compromise between the accuracy of computations and the computer time and memory requirements (Patankar, 1980; Douglass and

International Journal of Numerical Methods for Heat & Fluid Flow, Vol. 10 No. 1, 2000, pp. 6-46.

The authors are grateful to Dr I.V. Fryazinov for helpful discussions. R.P. Fedorenko acknowledges partial support of his work by the US Civil Research and Development Foundation (Grant No. RM2-157).

Ramshaw, 1994; Anderson, 1995; Fletcher, 1997; Roache, 1997; Coleman and Stern, 1998). Realistic engineering applications usually require the computation of complex flows in a three-dimensional geometry (e.g. Ramos, 1989; Webb, 1994). Moreover, the problem of flow computations is typically complicated by the need for coupled calculations of heat transfer, chemical composition, and possibly other processes such as transport of vibrational energy (Sazhin *et al.*, 1994). This can impose considerable strain on computer resources and so time-dependent solutions often turn out to be too expensive. It has, however, been established that in many cases a steady-state solution can lead to qualitatively misleading results. One of the most spectacular illustrations of this is the formation of the von Karman street, which could not be predicted if the flow around a bluff body is assumed to be steady (e.g. Durgin and Karlsson 1971; Belotzerkovskii *et al.*, 1988; Saffman, 1995; Panton, 1996). This well-known result has been widely ignored in many CFD applications. Only recently the problem surfaced in a paper by Zhang *et al.* (1997) which emphasised the importance of the transient effects on the performance of heat exchangers.

In this study we will focus our attention on one specific problem: the calculation of the two-dimensional flow around a square prism. This problem is closely related to the calculation of the effect of roughness on the flow in heat exchangers (Webb, 1994) or vortex generation in them (Fiebig, 1995; Xi *et al.*, 1995). In this paper the emphasis will be on the mathematical tools for solving this problem and detailed numerical results, rather than on the discussion of the applications of the method to specific engineering problems. The square cylinder was chosen because of the relative simplicity of the flow calculation around it and its applications to heat exchangers.

Numerical techniques to solve this problem can be divided into two main categories: discrete vortex methods (Leonard, 1980; Nagano *et al.*, 1982; Belotzerkovskii *et al.*, 1988; Sarpkaya, 1989, 1994, 1996), which are commonly employed at moderate and high Reynolds numbers, $\mathrm{Re} > 10^4$, and finite difference or finite element methods based on solving the Navier-Stokes equations (Davis and Moore, 1982; Davis *et al.*, 1984; Igarashi, 1984, 1985; Franke *et al.*, 1990; Tamura, 1990a, 1990b; Treidler, 1991; Okajima, 1982, 1990; Arnal *et al.*, 1991; Okajima *et al.*, 1992; Li and Humphrey, 1995; Wissink, 1995, 1997; Kondo and Yamada, 1995; Sohankar *et al.*, 1998; Hojo *et al.*, 1997). Since we are primarily interested in flows with $\mathrm{Re} \leq 500$ we will focus on the latter algorithms.

In this study we use an implicit finite-difference operator-splitting method employing the so-called primitive variables (velocity, pressure) and a staggered grid. This is a version of well-known SIMPLEC-like methods described, for example, by Patankar (1980). The main idea of this approach was suggested in the 1960s, and now these methods have reached their maturity. In this paper we present a full self-sufficient description of our method which we believe is particularly useful for readers not familiar with the background of the problem. Moreover, we combine the theoretical results referring to conservation properties and a priori estimates of discrete solutions.

Despite the considerable attention paid to the development of methods on collocated grids (e.g. Rhie and Chow, 1983; Shih *et al.*, 1989; Churbanov *et al.*, 1995; Vabishchevich *et al.*, 1996, 1997), the staggered grid remains the most popular choice in finite difference methods for solving incompressible Navier-Stokes equations in primitive variables. Our choice of the staggered grid approach is based on the results of systematic studies on the development and comparison of various numerical algorithms on different grids (Shih *et al.*, 1989; Vabishchevich *et al.*, 1996, 1997).

An operator-splitting technique, which is very similar to the SIMPLEC-type methods in time formulation, is used to derive the first-order scheme in time. This technique was theoretically investigated by Fryazinov *et al.* (1994) and Churbanov *et al.* (1995). A remarkable feature of this approach is that it does not require any boundary conditions for the pressure and provides a priori estimate of the discrete solution subject to the requirement that the spatial discrete operators meet some natural conditions. The estimate guarantees the boundedness of solutions of non-linear problems as well as stability for linearized problems. A priori estimates of such a type were earlier obtained by Ladysenskaya (1969) for a fully implicit method.

Almost all previous numerical studies have been based on the third-order upwind QUICK-type approximation for the convective terms (Leonard, 1979). In contrast, we employ the second-order central differences to approximate not only the viscous and pressure gradient terms but also the convective terms in the conservative form. Note that the same approximation was successfully used by Arakawa (1966), Fryazinov *et al.* (1994), Tafti (1996), and Zhang *et al.* (1997).

Our calculations showed that it is not necessary to use QUICK-type (Leonard, 1979) or implicit Fryazinov *et al.* (1994) or other more robust approximations when studying this particular problem. Below we show that an acceptable (from the smoothness standpoint) numerical solution can be obtained for the Reynolds numbers up to at least $\mathrm{Re} = 5 \cdot 10^5$ without noticeable increase in CPU time. Of course more robust approximations will need to be employed for approximation of the energy equation when heat transfer processes are involved.

It might be appropriate to point out that this approach does not contradict the conventional view on the stability properties of central differences. Stability analysis is usually applied to a stand-alone equation with explicitly treated approximations. For the two-stage operator-splitting procedure under consideration and the consistent set of implicit discrete equations, stability analysis is much more difficult and leads to a different result. The smoothing role of the second so-called pressure correction stage based on the continuity equation is clearly observed in the one-dimensional case. In this case it reverts any velocity field obtained at the first stage to a constant field, even if an oscillating solution was derived at the first stage.

In this paper we show that this method conserves not only mass and momentum, but also kinetic energy. The approximations which conserve

kinetic energy for convective terms were originally proposed by Arakawa (1966), and further developed by Fryazinov and Moiseenko (1981) and Fryazinov *et al.* (1994). Some useful properties of these approximations (namely, the ability to resolve the turbulent spectrum of a flow) were indicated by Tafti (1996). The property of conservation of the global kinetic energy is important for unsteady problems that are essentially dependent on the dissipation rate. Such flows occur in far wakes, in ventilation and fire problems with damping regimes under consideration. From the stability viewpoint this property is also important (Arakawa, 1966) since it provides an a priori estimate that guarantees the boundedness of a discrete solution (Fryazinov *et al.*, 1994; Churbanov *et al.*, 1995).

It is known that in most cases when studying numerically incompressible flows, most of the computational time is spent on solving the elliptic type pressure equation. So, we have paid special attention to an efficient solution of this algebraic problem. We used the multigrid approach, which is one of the most efficient algebraic tools for solving such problems to date (Botta *et al.*, 1997).

The multigrid method was developed by Fedorenko (1964, 1973) more than 30 years ago. Now this approach is well-known and widely used (Hackbusch, 1994; Wesseling, 1991). This method is associated with rather cumbersome book-keeping, but it is very attractive due to its very good asymptotic rate of $O(N)$. This means that the computational time is directly proportional to the number of unknowns in this method.

In this paper we present a new version of this method. A novelty of our approach is associated with a special manner used for formulating the algebraic equations on coarse grids. They are derived in such a way that, going in a backward direction from a coarse grid to a finer one, a correction of the pre-calculated solution yields an exact weak solution on the finer grid. The term "weak solution" is used here in the same sense as in finite element methods as a solution of a weighted residual equation as introduced below in Section 4.7.

The method was compared with an algebraic iterative solver, namely the modified incomplete Cholesky factorisation-conjugate gradient method (ICCG) (Saad, 1996), and was found to be more than twice as fast for the grid 401×321. It was also found to have a more promising asymptotic rate.

To solve the asymmetric momentum equations, a generalised conjugate gradient method ORTHOMIN(1) (Saad, 1996) is employed. In order to improve efficiency of the method, we use a preconditioning proposed by Henk and van der Vorst (1981). It allows efficient implementation of ORTHOMIN(1) and makes it robust and fast even in the case of non-symmetric matrix with large skew-symmetric part (at high Re numbers).

In Section 2 we give a brief review of the previous publications on numerical methods to solve the problem in question, while our mathematical formulation of the problem is given in Section 3. The numerical method used is described in detail in Section 4 and the results of our computations of the flow for $\mathrm{Re} = 100$,

200 and 500 are given in Section 5. Section 6 contains a comparison of the multigrid method with an iterative one. The main conclusions of the paper are summarised in Section 7.

2. Review of previous work

The problem of flow around rectangular prisms has been discussed by many authors (Nagano *et al.*, 1982; Davis and Moore, 1982; Davis *et al.*, 1984; Igarashi, 1984, 1985; Okajima, 1982, 1990; Franke *et al.*, 1990; Tamura, 1990a, 1990b; Treidler, 1991; Arnal *et al.*, 1991; Okajima *et al.*, 1992; Li and Humphrey, 1995; Wissink, 1995, 1997; Kondo and Yamada, 1995; Hojo *et al.*, 1997; Zhang *et al.*, 1997; Sohankar *et al.*, 1998). These studies can be classified according to the character of the flow (laminar or turbulent), Reynolds number, arrangement and cross-sectional shapes of the prisms, and whether a confined or a free-stream flow is considered. Most of the work reported in the literature is focused on laminar flow around a single prism immersed in a free-stream. In these studies the main objective was to determine integral quantities that characterise the aerodynamic behaviour of the prism (such as the drag and lift coefficients) as well as the Strouhal number. The Nusselt numbers are of particular interest when heat transfer is involved (Igarashi, 1985; Xi *et al.*, 1995; Zhang *et al.*, 1997).

Using the results of the previous experimental and numerical studies, the flow around a square prism may be briefly described as follows. At $\mathrm{Re} < \mathrm{Re}_{crit}$ the flow is steady, symmetric and stable and at $\mathrm{Re} > \mathrm{Re}_{crit}$ Hopf bifurcations occur (Wissink, 1995). Using the linearized Stuart-Landau equation for Hopf bifurcations (characteristic complex amplitude) (see, for example, Schumm *et al.*, 1994), Re_{crit} can be estimated to be equal to 51.2 ± 1.0, as was found by Sohankar *et al.* (1998).

As there is no received view on the sequence of flow regimes around a square prism as the Reynolds number increases, we can only cite results related to a flow around a circular cylinder. Experiments show that, for a relatively small range of Reynolds numbers (from $\mathrm{Re} = \mathrm{Re}_{crit}$ to about $\mathrm{Re} \approx 200$), a two-dimensional unsteady flow in the wake of a circular prism is observed, characterised by the well-known von Karman vortex street. At higher Re ($200 < \mathrm{Re} < 400$) a transition to a three-dimensional turbulent vortex street is expected (Karniadakis and Triantafyllou, 1992; Williamson, 1988, 1996; Blevins, 1977).

The numerical velocity-pressure based techniques employed to study the flow around the rectangular prism are summarised in Table I. Results of some important numerical studies based on the $\psi - \omega$ formulation and discrete vortex methods are briefly summarised by Sohankar *et al.* (1998).

In all these methods, except in the one used by Zhang *et al.* (1997), an implicit equation for pressure is derived using the SIMPLE-like approach. Zhang *et al.*, (1997) used the Chorin, Kim and Moin-type fractional-step approach. We recall that QUICKEST is an unsteady version of QUICK (see Leonard, 1979).

Authors	Year	Re	Grid	Method
Davis and More (1982); Davi *et al.* (1984)	1982, 1984	100-2,800	61×74	QUICKEST-type; approximation of momentum equation in space and time; staggered grid
Arnal *et al.* (1991)	1991	100, 500, 10^3	120×137	QUICK; explicit Runge-Kutta approximation of momentum equation in time; staggered grid
Okajima *et al.* (1992)	1992	$(1, 4, 7) \times 10^3$	Not specified	QUICKEST-type: approximation of momentum equation in space and time; staggered grid
Li and Humphrey (1995)	1995	$100\text{-}10^3$	100×55	QUICK; explicit Runge-Kutta approximation of momentum equation in time; staggered grid
Xi *et al.* (1995)	1995	180, 200	380×130	QUICK-type; fully implicit approximation of momentum equation in time
Kondo *et al.* (1995)	1995	10^4	1.4×10^4	Third-order upwind finite element method
Zhang *et al.* (1997)	1997	18-750	128×32, 512×256	Central differences; Chorin, Kim and Moin-type fractional-step method; an explicit Adams-Bashforth appoximation of spatial terms in time; staggered grid
Wissink (1997)	1997	10^4	400×400	Seventh-order upwind approximations in space; an explicit Adams-Bashforth approximation of momentum equation in time; staggered grid
Sohankar *et al.* (1998)	1998	45-200	348×224	QUICK; Crank-Nicolson approximation of momentum equation in time; non-staggered grid

Table I.
Numerical velocity-pressure based techniques for flow around rectangular prisms

All authors mentioned in Table I, except Okajima *et al.* (1992), used the laminar model of the flow. Okajima *et al.* (1992) compared the laminar and $k - \varepsilon$ turbulent models for $\mathrm{Re} = 10^3$ and found that the laminar model provides more adequate results than the turbulent model for this type of flow at this Reynolds number. Wissink (1997) used the direct numerical simulation approach to predict some characteristics of two-dimensional turbulent flow at $\mathrm{Re} = 10^4$.

These studies were aimed at obtaining flow parameters of practical interest such as the drag and lift coefficients as well as the Strouhal number. It should

be noted that in the early papers coarse grids with less than 100×100 nodes were used because of the low computer power available at that time. Hence, it was not possible to obtain grid-independent (within 1-2 per cent) solutions.

Only recently sufficiently fine grids were used by Arnal *et al.* (1991), Li and Humphrey (1995), Zhang *et al.* (1997) and Sohankar *et al.* (1998) to obtain reliable results at low Reynolds numbers ($\mathrm{Re} < 500$). Special attention was paid to the boundary conditions at the outlet. Sohankar *et al.* (1998) compared the so-called convective Sommerfeld and a Neumann boundary conditions. They have pointed out that at low Reynolds number the outlet boundary should be placed at more than $10d$ when the convective condition is used, and at more than $20d$ when the Neumann condition is used, where d is the width of the square prism.

In this paper predictions of the detailed characteristics of the flow around the prism at $\mathrm{Re} = 100$, 200, and 500 are presented. The case for $\mathrm{Re} = 500$ has been considered in more detail since results from the other two Reynolds numbers have already been reported by Sohankar *et al.* (1998). Comparison between our results and those obtained by Sohankar *et al.* (1998) has shown good agreement for the $\mathrm{Re} = 100$ and 200 cases. At $\mathrm{Re} = 500$ our results showed close correlations to those obtained by Arnal *et al.* (1991). However, the present study resulted in more accurate predictions of the flow parameters as well as revealing some new features of the problem. These features refer to an existence of two transient fully periodic flows that are mirror symmetric to each other.

Moreover, a detailed picture of vortex formation and shedding over a period is presented for this complex flow. In contrast to most previously reported results, a detailed picture of the flow is presented not only in the vicinity of the prism but also in the wake. The absence of the numerical dissipation of kinetic energy incorporated in the method has enabled a non-damped vortical flow in the wake to be obtained.

It should be noted that, even though two-dimensional numerical results at $\mathrm{Re} = 500$ do not strictly correspond to actual three-dimensional flow (see Zhang *et al.*, 1997), these results are interesting in their own right. Owing to its simple geometry, rich physical phenomena and relevant practical applications this problem may be used as a CFD benchmark problem.

3. Formulation of the problem

Laminar flow around a square prism immersed in a free-stream is considered. This flow is assumed to be two-dimensional, unsteady, incompressible and viscous. The relevant continuity and Navier–Stokes equations can be written in dimensionless form as:

$$\nabla \cdot \mathbf{v} = 0, \mathbf{x} \in \Omega, t > 0, \tag{1}$$

$$\frac{\partial \mathbf{v}}{\partial t} + (\mathbf{v} \cdot \nabla)\mathbf{v} + \nabla p = \frac{1}{\mathrm{Re}} \nabla^2 \mathbf{v}, \mathbf{x} \in \Omega, t > 0, \tag{2}$$

where the following dimensionless parameters are used: t is the dimensionless time, normalised by d/V_∞, $\mathbf{v}$ is the dimensionless velocity vector, $\mathbf{v} = (v_1, v_2)$, normalised by V_∞, p is the dimensionless pressure, normalised by ρV_∞^2, ρ is density. The Reynolds number Re is defined by $V_\infty d/\nu$, where ν is the kinematic viscosity. The computational domain, notation and boundary conditions are shown in Figure 1. No-slip boundary conditions ($\mathbf{v} = 0$) are imposed on the surface of the prism. Symmetry boundary conditions are used on the upper and lower boundaries and the flow is undisturbed and uniform at the inlet. At the outlet the boundary conditions are specified by zero-gradient conditions for the velocity components, $\partial \mathbf{v}/\partial x_1 = 0$.

Sometimes the so-called convective Sommerfeld condition $\partial v_1/\partial t + c(\partial v_1/\partial x_1) = 0$ is used at the outlet boundary (see Arnal *et al.*, 1991; Li and Humphrey, 1995; Hojo *et al.*, 1997; Sohankar *et al.*, 1998). It allows the vortical flow structures to pass through the outlet boundary without reflecting waves. We did not face this problem in our computations. We believe that this may be due to the fact that our discrete equations are consistent with the differential ones regarding the properties of the operators, although this was not investigated in this paper. Besides, the outlet boundary was placed sufficiently far from the prism so that it had little influence on the flow near the prism. Note that the convective and Neumann boundary conditions lead to the same results if the distance from the prism to outlet boundary is more than about 20d (Sohankar *et al.*, 1998).

4. Numerical method

Although the SIMPLE-like approach and its modifications are well-known (Patankar, 1980), it seems to be useful to present a full, self-sufficient description of the method. Besides, here we collected related theoretical results referring to conservation properties of discrete equations and a priori estimates of their solution.

An implicit finite-difference method to solve equations (1) and (2) is based on employing primitive variables (velocity, pressure) and non-uniform staggered grids alongside with an operator-splitting technique. The operator-splitting technique is presented following Churbanov *et al.* (1995). Kinetic energy conservation in the central differences method for convective terms is presented following from Arakawa's (1966) and Fryazinov *et al.*'s (1994)

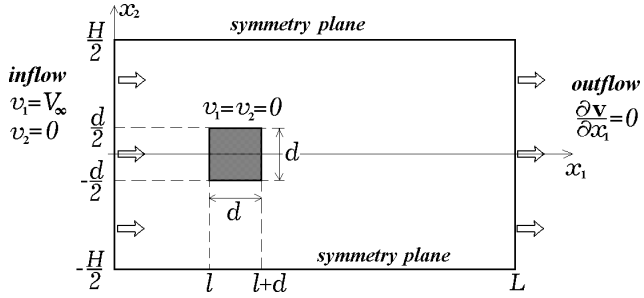

Figure 1. Computational domain and boundary conditions

approach. Since the latter approach is not widely known, we briefly discuss it and provide related algebraic manipulations in Appendix A. Note that this aproach was originally developed for a bounded problem. Here it is applied to the problem with open boundaries and a body immersed in the flow.

A new feature of our numerical analysis is the modification of the multigrid approach which refers to the formulation of an algebraic problem on a coarse grid when going from a fine grid to a coarse one. Some pre-calculated solutions are obtained for each grid at this stage. At the second stage when going backwards from the coarsest grid to the finest one, corrections of the pre-calculated solutions produce exact weak solutions on each grid as shown below in Section 4.7.

4.1 Staggered grid and notation

To simplify the presentation, we will focus our attention mainly on uniform grids. Necessary comments on approximations for a non-uniform grid are given in Appendix B.

Let us introduce a uniform grid with spacings $h_1 = L/N_1$ and $h_2 = H/N_2$ in the domain in question $\Omega = \left\{(x_1, x_2) | 0 < x_1 < L, -\frac{1}{2}H < x_2 < \frac{1}{2}H\right\}$. Let ω_{v_1}, ω_{v_2} and ω_p be the sets of internal points for the velocity components and pressure:

$$\omega_{v_1} = \{(x_{1i}, x_{2j}) | x_{1i} = ih_1, x_{2j} = (j - \tfrac{1}{2})h_2 - \tfrac{1}{2}H, \\ i = 1, 2, \ldots, N_1 - 1, j = 1, 2, \ldots, N_2\},$$

$$\omega_{v2} = \{(x_{1i}, x_{2j}) | x_{1i} = (i - \tfrac{1}{2})h_1, x_{2j} = jh_2 - \tfrac{1}{2}H \\ i = 1, 2, \ldots, N_1, j = 1, 2, \ldots, N_2 - 1\},$$

$$\omega_p = \{(x_{1i}, x_{2j}) | x_{1i} = (i - \tfrac{1}{2})h_1, x_{2j} = (j - \tfrac{1}{2})h_2 - \tfrac{1}{2}H, \\ i = 1, 2, \ldots, N_1, j = 1, 2, \ldots, N_2\}$$

Denote by $\partial\omega_{v_1}$ and $\partial\omega_{v_2}$ the sets of boundary points, and by $\bar{\omega}_{v_1}$ and $\bar{\omega}_{v_2}$ the sets of all points for the corresponding velocity components, $\bar{\omega}_{v_1} = \omega_{v_1} \cup \partial\omega_{v_1}$, $\bar{\omega}_{v_2} = \omega_{v_2} \cup \partial\omega_{v_2}$ (see Figure 2). Note that the points lying on the prism surface belong to the sets of boundary points, and points inside the prism do not belong to any set.

Let us introduce, for later use, interpolated values of the velocity components, (see Figure 2). The interpolated velocity components at the centres of cells are defined as

$$\dot{v}_{1i,j} = \tfrac{1}{2}(v_{1i,j} + v_{1i-1,j}), \dot{v}_{2i,j} = \tfrac{1}{2}(v_{2i,j} + v_{2i,j-1}), \mathbf{x} \in \omega_p, \tag{3}$$

and the interpolated values at the corner points of cells are defined as

$$\hat{v}_{1i,j} = \tfrac{1}{2}(v_{1i,j} + v_{1i,j+1}), \hat{v}_{2i,j} = \tfrac{1}{2}(v_{2i,j} + v_{2i+1,j}), \tag{4}$$

$$i = 0, 1, \ldots, N_1, j = 0, 1, \ldots, N_2.$$

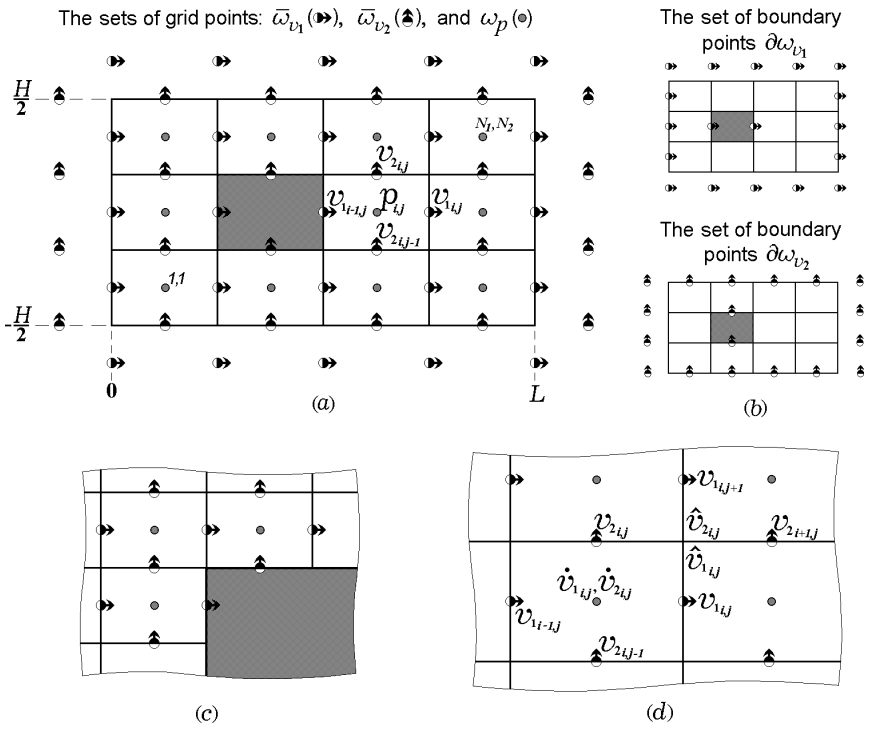

Figure 2.
(a) staggered computational grid in the domain including the boundary points; (b) the sets of boundary points; (c) the grid near prism; and (d) location of interpolated velocity components

Let us use the following notation for the first-order forward, backward and the second-order central differences with respect to x_1

$$(u_{x_1^+})_{i,j} = \frac{u_{i+1,j} - y_{i,j}}{h_1}, (u_{x_1^-})_{i,j} = \frac{u_{i,j} - u_{i-1,j}}{h_1}, (u_{x_1^\circ})_{i,j} = \frac{u_{i+1,j} - u_{i-1,j}}{2h_1}, \quad (5)$$

and similar notation for differences with respect to x_2.

4.2 Spatial discretization

Let us introduce the second-order central differences to approximate the velocity divergence in the continuity equation, the pressure gradient, and the convective and diffusion terms in the momentum equation. Denoting by div_h, grad_h, $\boldsymbol{C}_h(\mathbf{v})$ and $\boldsymbol{D}_h$ corresponding difference operators, we define them as follows:

$$\nabla \cdot \mathbf{v} \approx (\mathrm{div}_h \mathbf{v})_{i,j} = \frac{v_{1i,j} - v_{1i-1,j}}{h_1} + \frac{v_{2i,j} - v_{2i,j-1}}{h_2}, \mathbf{x} \in \omega_p, \quad (6)$$

$$\nabla p \approx \mathrm{grad}_h p = ((\mathrm{grad}_h p)_1, (\mathrm{grad}_h p)_2), \quad (7)$$

where

$$(\mathrm{grad}_h p)_{1i,j} = \frac{p_{i+1,j} - p_{i,j}}{h_1}, \mathbf{x} \in \omega_{v_1}, (\mathrm{grad}_h p)_{2i,j} = \frac{p_{i,j+1} - p_{i,j}}{h_2}, \mathbf{x} \in \omega_{v_2}, \quad (8)$$

$$\nabla \cdot (\mathbf{v}v_1) \approx C_h(\mathbf{v})v_1, \qquad \mathbf{x} \in \omega_{v_1}, \tag{9}$$

where

$$(C_h(\mathbf{v})v_1)_{i,j} = \frac{\left(\frac{1}{2}(v_{1i+1,j} + v_{1i,j})\right)^2 - \left(\frac{1}{2}(v_{1i,j} + v_{1i-1,j})\right)^2}{h_1} + \frac{\frac{1}{4}(v_{1i,j+1} + v_{1i,j})(v_{2i+1,j} + v_{2i,j}) - \frac{1}{4}(v_{1i,j} + v_{1i,j-1})(v_{2i+1,j-1} + v_{2i,j-1})}{h_2}, \tag{10}$$

$$\nabla \cdot (\mathbf{v}v_2) \approx C_h(\mathbf{v})v_2, \qquad \mathbf{x} \in \omega_{v_2}, \tag{11}$$

where

$$(C_h(\mathbf{v})v_2)_{i,j} = \frac{\frac{1}{4}(v_{1i,j+1} + v_{1i,j})(v_{2i+1,j} + v_{2i,j}) - \frac{1}{4}(v_{1i-1,j+1} + v_{1i-1,j})(v_{2i,j} + v_{2i-1,j})}{h_1} + \frac{\left(\frac{1}{2}(v_{2i,j+1} + v_{2i,j})\right)^2 - \left(\frac{1}{2}(v_{2i,j} + v_{2i,j-1})\right)^2}{h_2}. \tag{12}$$

Note that the conservative form of the convective terms is employed here.

Approximating viscous terms, modified differences are used at grid points in the vicinity of the prism or, more specifically, at v_1-grid points near the top and bottom prism surfaces and at v_2-grid points near the left and right prism surfaces (see Figure 3). For these cells the one-side second-order differences are used to approximate fluxes (the friction force) on the prism surface. The zero values of velocity on the prism surfaces are taken into account. We introduce ω_T and ω_B as the subsets of the v_1-grid points adjacent to the top and bottom prism surfaces, and ω_L, ω_R as the subsets of the v_2-grid points adjacent to the left and right prism surfaces. Now define the discrete viscous operator as follows

$$\nabla^2 \mathbf{v} \approx D_h \mathbf{v} = \left((D_{x_1}^{v_1} + D_{x_2}^{v_1})v_1, (D_{x_1}^{v_2} + D_{x_2}^{v_2})v_2 \right), \tag{13}$$

where $D_{x_\beta}^{v_\alpha}$ approximates the second-order derivative of v_α with respect to coordinate x_β.

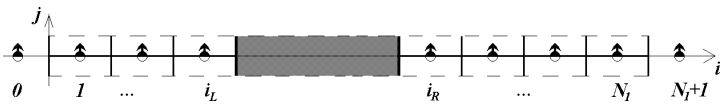

Figure 3.
The v_2 grid points lying along an x_1-line that passes through the prism. Here $x_{i_L,j} \in \omega_L$ and $x_{i_R,j} \in \omega_R$; see operator D_{x1}^{v2}

$$\left(D_{x_1}^{v_1} v_1\right)_{i,j} = \frac{v_{1i+1,j} - 2v_{1i,j} + v_{1i-1,j}}{h_1^2}, \mathbf{x} \in \omega_{v_1}, \tag{14}$$

$$\left(D_{x_2}^{v_1} v_1\right)_{i,j} = \begin{cases} \dfrac{v_{1i,j+1} - 2v_{1i,j} + v_{1i,j-1}}{h_2^2}, & \mathbf{x} \in \omega \mathrm{v1} \backslash (\omega \mathrm{T} \cup \omega \mathrm{B}), \\ \dfrac{(\frac{1}{3} v_{1i,j-1} - 3v_{1i,j}) - (v_{1i,j} - v_{1i,j-1})}{h_2^2}, & \mathbf{x} \in \omega \mathrm{B}, \\ \dfrac{(v_{1i,j+1} - v_{1i,j}) - (3v_{1i,j} - \frac{1}{3} v_{1i,j+1})}{h_2^2}, & \mathbf{x} \in \omega \mathrm{T}, \end{cases} \tag{15}$$

$$\left(D_{x_1}^{v_2} v_2\right)_{i,j} = \begin{cases} \dfrac{v_{2i+1,j} - 2v_{2i,j} + v_{2i-1,j}}{h_1^2}, & \mathbf{x} \in \omega \mathrm{v2} \backslash (\omega \mathrm{L} \cup \omega \mathrm{R}), \\ \dfrac{(\frac{1}{3} v_{2i-1,j} - 3v_{2i,j}) - (v_{2i,j} - v_{2i-1,j})}{h_1^2}, & \mathbf{x} \in \omega \mathrm{L}, \\ \dfrac{(v_{2i+1,j} - v_{2i,j}) - (3v_{2i,j} - \frac{1}{3} v_{2i+1,j})}{h_1^2}, & \mathbf{x} \in \omega \mathrm{R}, \end{cases} \tag{16}$$

$$\left(D_{x_2}^{v_2} v_2\right)_{i,j} = \frac{v_{2i,j+1} - 2v_{2i,j} + v_{2i,j-1}}{h_2^2}, \mathbf{x} \in \omega_{v_2}. \tag{17}$$

Using definitions (3)-(4) for interpolated velocities ($\dot{v}_i$ and $\hat{v}_i$, $i = 1, 2$), and (5) for the forward ($(v_i)_{x_j^+}$), backward ($(v_i)_{x_j^-}$) and central ($(v_i)_{\mathring{x}_j}$, $i = 1, 2$, $j = 1, 2$) differences, we can write the following semi-discrete (continuous in time and discrete in space) equations that approximate (1) and (2):

$$(v_1)_{x_1^-} + (v_2)_{x_2^-} = 0, \mathbf{x} \in \omega_p, t > 0, \tag{18}$$

$$\frac{\partial v_1}{\partial t} + (\dot{v}_1^2)_{x_1^+} + (\hat{v}_1 \hat{v}_2)_{x_2^-} + p_{x_1^+} = \frac{1}{\mathrm{Re}} \left(D_{x_1}^{v_1} v_1 + D_{x_2}^{v_1} v_1\right), \mathbf{x} \in \omega_{v_1}, t > 0, \tag{19}$$

$$\frac{\partial v_2}{\partial t} + (\hat{v}_1 \hat{v}_2)_{x_1^-} + (\dot{v}_2^2)_{x_2^+} + p_{x_2^+} = \frac{1}{\mathrm{Re}} \left(D_{x_1}^{v_2} v_2 + D_{x_2}^{v_2} v_2\right), \mathbf{x} \in \omega_{v_2}, t > 0. \tag{20}$$

4.3 Boundary conditions

Let us approximate the boundary condition $\partial \mathbf{v} / \partial x_1 = 0$ at the outlet as

$$(v_1)_{x_1^-} = 0, i = N_1, j = 1, 2, \ldots, N_2, (v_2)_{x_1^-} = 0, i = N_1 + 1,$$
$$j = 1, 2, \ldots, N_2 - 1,$$

Substituting the first condition into the continuity equation (18), we obtain $(v_2)_{x_2^-} = 0,\ i = N_1,\ j = 1, 2, \ldots, N_2$. Taking into account the symmetry conditions at the top and bottom boundaries, $v_2 = 0$ at $j = 0$ and $j = N_2$, this equation gives $v_2 = 0, i = N_1, j = 0, 1, 2, \ldots, N_2$.

Using this modification of the boundary conditions at the outlet, we can write the following boundary conditions for the problem at the inlet:
at the inlet:

$$v_{1i,j} = 1, i = 0, j = 1, 2, \ldots, N_2, v_{2i,j} = 0, i = 0, j = 0, 1, \ldots, N_2, \tag{21}$$

at the outlet:

$$(v_1)_{x_1^-} = 0, i = N_1, j = 1, 2, \ldots, N_2, v_{2i,j} = 0, i = N_1, N_1 + 1, \quad j = 0, 1, \ldots, N_2, \tag{22}$$

at the symmetry plane $x_1 = \frac{1}{2}H$:

$$(v_1)_{x_2^-} = 0, i = 0, 1, \ldots, N_1, j = N_2 + 1, v_{2i,j} = 0, i = 0, 1, \ldots, N_2 + 1, \quad j = N_2, \tag{23}$$

at the symmetry plane $x_1 = -\frac{1}{2}H$:

$$(v_1)_{x_2^+} = 0, i = 0, 1, \ldots, N_1, j = 0, v_{2i,j} = 0, i = 0, 1, \ldots, N_2 + 1, j = 0, \tag{24}$$

at the prism surface:

$$v_1 = 0, v_2 = 0. \tag{25}$$

It should be noted that there is no need to impose any boundary conditions for the pressure. A closed discrete problem for pressure is derived via algebraic transformations of the discretized continuity and momentum equations and the velocity boundary conditions as discussed below in Section 4.4.

4.4 Time discretization

An operator-splitting technique is well-accepted in CFD. It is used here to resolve efficiently the pressure-velocity coupling problem. The approach used in our paper is similar to the SIMPLEC-type methods in time formulation. We describe it following Churbanov *et al.* (1995). Let us split the operators of the momentum equations into two parts associated with velocity and pressure, and rewrite semi-discrete equations (19) and (20) as a single equation for $\mathbf{v}$

$$\frac{\partial \mathbf{v}}{\partial t} + (\mathsf{A}_1 + \mathsf{A}_2)\mathbf{v} = 0, t > 0, \tag{26}$$

where the formal notation A_1 and A_2 is used for

$$\mathsf{A}_1 = \mathsf{C}_h(\mathbf{v}) + \mathsf{D}_h, (\mathsf{A}_1\mathbf{v} \cdot \mathbf{v}) \geq 0, \tag{27}$$

$$\mathsf{A}_2\mathbf{v} = \mathrm{grad}_h p, \qquad (\mathsf{A}_2\mathbf{v}\cdot\mathbf{v}) = 0. \tag{28}$$

Let superscripts n and $n+1$ indicate the successive time levels and $n+\frac{1}{2}$ denotes the intermediate values. Now we can write the following additive scheme for (26)

$$\frac{\mathbf{v}^{n+1/2}-\mathbf{v}^n}{\tau} + A_1\mathbf{v}^{n+1/2} + A_2\mathbf{v}^n = 0, \tag{29}$$

$$\frac{\mathbf{v}^{n+1}-\mathbf{v}^n}{\tau} + A_1\mathbf{v}^{n+1/2} + A_2\mathbf{v}^{n+1} = 0. \tag{30}$$

This is the limiting case of the more general factorized scheme described by Churbanov *et al.* (1995). Without taking into account the specific meanings of the operators, this has the form of the well-known Douglas-Rachford scheme in the two-dimensional case.

We use the convective terms in the form $\mathsf{C}_h(\mathbf{v}^n)\mathbf{v}^{n+1/2}$ that is linear with respect to $\mathbf{v}^{n+1/2}$, and add the fully implicit, in time, continuity equation

$$\mathrm{div}_h\mathbf{v}^{n+1} = 0 \tag{31}$$

to (29) and (30). This scheme takes a form that is very similar to the SIMPLEC-type pressure correction algorithm with respect to time discretization. It has first order accuracy with respect to time.

It is logical to use the notation of linear difference operator theory (Marchuk, 1982; Samarskii, 1989) as some ideas of this well-established theory are used to obtain a priori estimates.

Following Veldman (1990) and Churbanov *et al.* (1995), an accurate approach is employed to implement the scheme (29)-(31) along with the boundary conditions (21)-(25). First, the continuity and momentum equations are discretized, then the closed discrete formulation for pressure is derived by means of algebraic transformations of the original grid equations along with discrete boundary conditions for velocity. Thus algebraically equivalent equations are used for the calculations instead of the originally derived ones. This approach allows us to avoid any boundary conditions for the pressure (Veldman, 1990). Note that the application of the discrete equations (29)-(31) and boundary conditions together is a rather important point in obtaining closed final algebraic equations. In this case the boundary conditions (21)-(25) are used for velocities at time levels $\mathbf{v}^{n+1}$ as well as intermediate velocities $\mathbf{v}^{n+\frac{1}{2}}$. The second important point in obtaining the closed final problem is that the number of pressure points needs to be equal to the number of discrete continuity equations (31).

Having subtracted (30) from (29), after simple manipulations, we obtain:

$$\mathbf{v}^{n+1} = \mathbf{v}^{n+1/2} - \tau\cdot\mathrm{grad}_h(p^{n+1}-p^n). \tag{32}$$

This equation is used in the calculations instead of (30).

Substituting (32) and the boundary conditions for $\mathbf{v}^{n+1}$ into the continuity equation (31), we get an algebraic equation for pressure. The pressure equation is used in the calculations instead of the continuity equation (31).

4.5 Final form of the algorithm

Using interpolated velocities $\hat{v}_i$ and $\hat{v}_i$, $i = 1, 2$ defined by (3), (4), and notation $(v_i)_{x_i^+}$, $(v_i)_{x_i^-}$ and $(v_i)_{\mathring{x}_j}$ for the corresponding forward, backward and central differences defined by (5), the final discretized equations can be written as

(i) evaluation of the intermediate velocity,

$$\frac{v_1^{n+\frac{1}{2}} - v_1^n}{\tau} + (\hat{v}_1^n \hat{v}_1^{n+\frac{1}{2}})_{x_1^+} + (\hat{v}_2^n \hat{v}_1^{n+\frac{1}{2}})_{x_2^-} - \frac{1}{\mathrm{Re}}\left((v_1^{n+\frac{1}{2}})_{x_1^- x_1^+} + \mathsf{D}_{x_2}^{v_1} v_1^{n+\frac{1}{2}}\right) + p_{x_1^+}^n = 0, \mathbf{x} \in \omega_{v_1}, \tag{33}$$

$$\frac{v_2^{n+\frac{1}{2}} - v_2^n}{\tau} + (\hat{v}_1^n \hat{v}_2^{n+\frac{1}{2}})_{x_1^-} + (\hat{v}_2^n \hat{v}_2^{n+\frac{1}{2}})_{x_2^+} - \frac{1}{\mathrm{Re}}\left(\mathsf{D}_{x_1}^{v_2} v_2^{n+\frac{1}{2}} + (v_2^{n+\frac{1}{2}})_{x_2^- x_2^+}\right) + p_{x_2^+}^n = 0, \mathbf{x} \in \omega_{v_2}, \tag{34}$$

(ii) calculation of the pressure correction,

$$(\kappa_1 \delta p_{x_1^+})_{x_1^-} + (\kappa_2 \delta p_{x_2^+})_{x_2^-} = \frac{1}{\tau}\left((v_1^{n+\frac{1}{2}})_{x_1^-} + (v_2^{n+\frac{1}{2}})_{x_2^-}\right), \quad i = 1, 2, \ldots, N_1 - 1, \quad j = 1, 2, \ldots, N_2, \tag{35}$$

$$\delta p_{N_1, j} = 0, \quad j = 1, 2, \ldots, N_2, \tag{46}$$

where κ_1 and κ_2 are auxiliary coefficients located at v_1- and v_2-grid points respectively, $\kappa_1 \in \mathcal{H}_{v1}, \kappa_2 \in \mathcal{H}_{v2}$. They are introduced to shorten the formulation of the problem, and are defined as

$$\kappa_{1i,j} = \begin{cases} 0 & \text{at grid points lying at inlet and prism surface,} \\ 1 & \text{at all other points,} \end{cases}$$

$$\kappa_{2i,j} = \begin{cases} 0 & \text{at grid points lying at bottom and top boundaries and prism surface,} \\ 1 & \text{at all other points,} \end{cases}$$

(iii) evaluation of the velocity and pressure at the next time-level,

$$v_1^{n+1} = v_1^{n+\frac{1}{2}} - \tau \delta p_{x_1^+}, \mathbf{x} \in \omega_{v_1}, v_2^{n+1} = v_2^{n+\frac{1}{2}} - \tau \delta p_{x_2^+}, \mathbf{x} \in \omega_{v_2}, \tag{37}$$

$$p^{n+1} = p^n + \delta p, \mathbf{x} \in \omega_p, \tag{38}$$

with boundary conditions (21)-(25) for both intermediate velocities $\mathbf{v}^{n+\frac{1}{2}}$ and velocities $\mathbf{v}^{n+1}$; and initial conditions:

$$v_1^0 = 1, \mathbf{x} \in \omega_{v_1}, v_2^0 = 0, \mathbf{x} \in \omega_{v_2}. \tag{39}$$

4.6 Mass, momentum and kinetic energy conservation. A priori estimate

Let us display conservative properties and a priori estimates of the semi-discrete equations (18)-(20) and the final discrete equations (33)-(38).

As the divergence form of operators is used in the continuity and momentum equations it is easy to obtain the discrete mass and momentum conservation properties. Multiplying the continuity equation (19) by $h_1 h_2$ and summing it over ω_p immediately yields mass conservation. This means that the total rate of flow through the boundary is equal to zero.

Repeating the same operations for the momentum equations (19) and (20), one obtains the discrete momentum conservation property. This means that for a problem with zero velocity at all boundaries the total discrete momentum (in the whole domain) changes only due to the friction force at the boundaries.

Now we show that discrete equations (18)-(20) also conserve kinetic energy, i.e. that the kinetic energy in the whole domain changes only due to positive dissipation, which is solely defined by the viscous term.

Strictly speaking, discrete equations should be considered along with boundary conditions when integral properties of a problem are under consideration. First, we obtain results for a problem with zero velocity at the boundary (zero Dirichlet conditions) and then present only the final results for the channel-type problem considered (that is the problem with both Dirichlet and Neumann conditions at boundary). Below we consider solenoidal discrete vector functions $\mathbf{v}$. A vector function is called solenoidal if it satisfies a discrete continuity equation $\mathrm{div}_h \mathbf{v} = 0, \mathbf{x} \in \omega_p$.

Let us consider the finite-dimensional Hilbert space of v_1-grid functions $\mathcal{H}_{v_1}$ with the scalar product

$$(u \cdot w)_{v_1} = \sum_{\mathbf{x} \in \omega_{v_1}} u(\mathbf{x}) w(\mathbf{x}) h_1 h_2, u, w \in \mathcal{H}_{v_1},$$

and the space $\mathcal{H}_{v_2}$ of v_2-grid functions with similarly defined scalar product $(u \cdot w)_{v_2}$.

Define the Hilbert space $\mathcal{H}^2$ as the direct sum $\mathcal{H}^2 = \mathcal{H}_{v_1} \oplus \mathcal{H}_{v_2}$ with the corresponding scalar product

$$(\mathbf{u} \cdot \mathbf{w}) = \sum_{\alpha=1}^{2} (u_\alpha, w_\alpha)_{v_\alpha} \quad \text{and the norm} \quad \|\mathbf{u}\| = (\mathbf{u}, \mathbf{u})^{1/2}.$$

Finally define the Hilbert space $\mathcal{H}^2_{sol}$ as the subspace of solenoidal vector functions of the space $\mathcal{H}^2$ with the same scalar product.

The kinetic energy conservation and an existence of a priory estimate are closely connected with each other. Both they are based on the following properties of the discrete operators:

$$(\mathrm{grad}_h p \cdot \mathbf{w}) = 0, \tag{40}$$

$$(\mathsf{C}_h(\mathbf{w})\mathbf{v} \cdot \mathbf{v}) = 0, \tag{41}$$

$$(-\mathsf{D}_h\mathbf{v} \cdot \mathbf{v}) \geq 0 \tag{42}$$

for any $\mathbf{w} \in \mathcal{H}^2_{sol}$ and $\mathbf{v} \in \mathcal{H}^2$ with zero values at the boundary. Notice that in (40)-(42) the solenoidality is required only for vector function $\mathbf{w}$. Operators grad_h and $C_h(\mathbf{w})$ that satisfy (40) and (41) are said to be skew-symmetric.

From the physical point of view, these properties mean that the discrete pressure gradient and convective terms do not contribute to the kinetic energy; and the viscous term leads to the dissipation of kinetic energy.

The proofs of properties (40)-(42) for the operators (6)-(17) introduced above are given in Appendix A.

To receive the kinetic energy conservation property and the simplest a priori estimate for a solution of problem (18)-(20) with zero values at the boundary, let us multiply (19) by v_1, and (20) by v_2, and then take the scalar product in $\mathcal{H}^2_{sol}$:

$$\frac{\partial}{\partial t}\left(\tfrac{1}{2}\|\mathbf{v}\|^2\right) + (\mathsf{C}_h(\mathbf{v})\mathbf{v} \cdot \mathbf{v}) + (\mathrm{grad}_h p \cdot \mathbf{v}) = \frac{1}{\mathrm{Re}}(\mathsf{D}_h\mathbf{v} \cdot \mathbf{v}).$$

Using the above-mentioned basic properties (40)-(42), we obtain the kinetic energy conservation property

$$\frac{\partial \mathrm{E}_{kin}}{\partial t} = -\mathcal{N}_{diss},$$

where E_{kin} is the total kinetic energy, $\mathrm{E}_{kin} = \frac{1}{2}\|\mathbf{v}\|^2$, and $\mathcal{N}_{diss}$ is the total viscous dissipation, $\mathcal{N}_{diss} = -\frac{1}{\mathrm{Re}z}(D_h\mathbf{v} \cdot \mathbf{v}) \geq 0$. From this equation it follows that $\partial(\|\mathbf{v}\|)/\partial t \leq 0$. Using this inequality, one can derive the following estimate (Fryazinov *et al.*, 1994; Churbanov *et al.*, 1995):

$$\|\mathbf{v}(\mathbf{x}, t)\| \leq \|\mathbf{v}(\mathbf{x}, 0)\|. \tag{43}$$

Derivation of a priori estimates becomes much more complex when an operator-splitting technique is employed to solve the semi-discrete equations (18)-(20). To obtain an a priori estimate for the solution of the operator-splitting method (29)-(31), Churbanov *et al.* (1995) used some of the approaches of linear difference operator theory (Marchuk, 1982; Samarskii, 1989). It is well-known (see Samarskii, 1989) that in the linear case the scheme (29), (30) is unconditionally stable if $A_1 \geq 0$ and $A_2 \geq 0$. In the general non-linear case this leads to the following estimate (Churbanov *et al.*, 1995):

$$\|(E + \tau\mathsf{A}_2)\mathbf{v}^{n+1}\| \leq \|(E + \tau\mathsf{A}_2)\mathbf{v}^n\|. \tag{44}$$

Moreover, Fryazinov *et al.* (1994) and Churbanov *et al.* (1995) have shown that for a non-linear scheme (29)-(31) with properties (40)-(42) the following a priori estimate holds true:

$$\|\mathbf{v}^{n+1}\| \le \left(\|\mathbf{v}^0\|^2 + \tau^2 \|\mathrm{grad}_h p^0\|^2\right)^{1/2}, \tag{45}$$

where $\mathbf{v}^0 = \mathbf{v}(\mathbf{x}, 0)$ and $p^0 = p(\mathbf{x}, 0)$ are initial conditions. This can be proved based on the derivation presented by Churbanov *et al.* (1995). We emphasise that these estimates are valid only for a problem with zero Dirichlet boundary conditions for velocity.

The estimate (45) guarantees the boundedness of the discrete solution of the operator-splitting method (33)-(38) for the non-linear problem. It also provides unconditional stability of the solution with respect to initial data but only for linearized problems.

In the general non-linear case it provides unconditional stability for the trivial (zero) solution only.

Finally, omitting rather cumbersome manipulation we present the kinetic energy conservation property for the considered channel-type problem, i.e. for the semi-discrete equations (18)-(20) with boundary conditions (21)-(25). In this case we obtain the following equation:

$$\frac{\partial \mathrm{E}_{kin}}{\partial t} + \sum_{j=1}^{N_2} \left(-\frac{(\dot{v}_1)_{1,j}(v_1)_{0,j}(v_1)_{1,j}}{2} - p_{1,j}(v_1)_{0,j} + \frac{(v_1)^3_{N_1,j}}{2} + p_{N_1,j}(v_1)_{N_1,j} \right) \tag{46}$$
$$h_2 = -\mathcal{N}_{diss},$$

that is fully consistent with the corresponding equation (with integrals instead of sums) for the continuous problem (1), (2). It means that the changes in total kinetic energy are due to:

- the difference of its inflow and outflow fluxes;
- the work done by the pressure force; and
- the viscous dissipation.

We suspect that it is possible to obtain an a priori estimate of a discrete solution in this case too but this will require special investigation.

It should be noted that the mass and momentum conservation properties hold true for the final discrete equations (33)-(38) too.

The total kinetic energy is not conserved exactly by these equations due to splitting approximations in time when employing the operator-splitting technique.

All these results are applicable to non-uniform grids provided that the interpolated velocities (4) are defined as shown in Appendix B.

4.7 Multigrid method

Since most of the computational time is spent on solving the elliptic type pressure correction equation (35), we have paid special attention to the efficient solution of this problem. The multigrid method has been used for this purpose (Fedorenko, 1964, 1973).

The multigrid method is associated with rather cumbersome "book-keeping", but it is very attractive due to its very good asymptotic rate of $O(N)$. This means that in this method the computational time is directly proportional to the number of grid points. This is consistent with the results of computations shown later in this paper.

As the multigrid approach is well-known (Hackbusch, 1994; Wesseling, 1991), we will focus our attention only on the new features and make some comments that allow us to understand the method and use it efficiently.

Generally speaking, the multigrid approach is associated with solving systems of algebraic equations on a sequence of grids moving from the finest grid to coarser and coarser grids and then backwards from the coarsest grid to the finest one. A general scheme of the algorithm, which we have used, can be presented as shown in Figure 4. We use the following notation: S is a

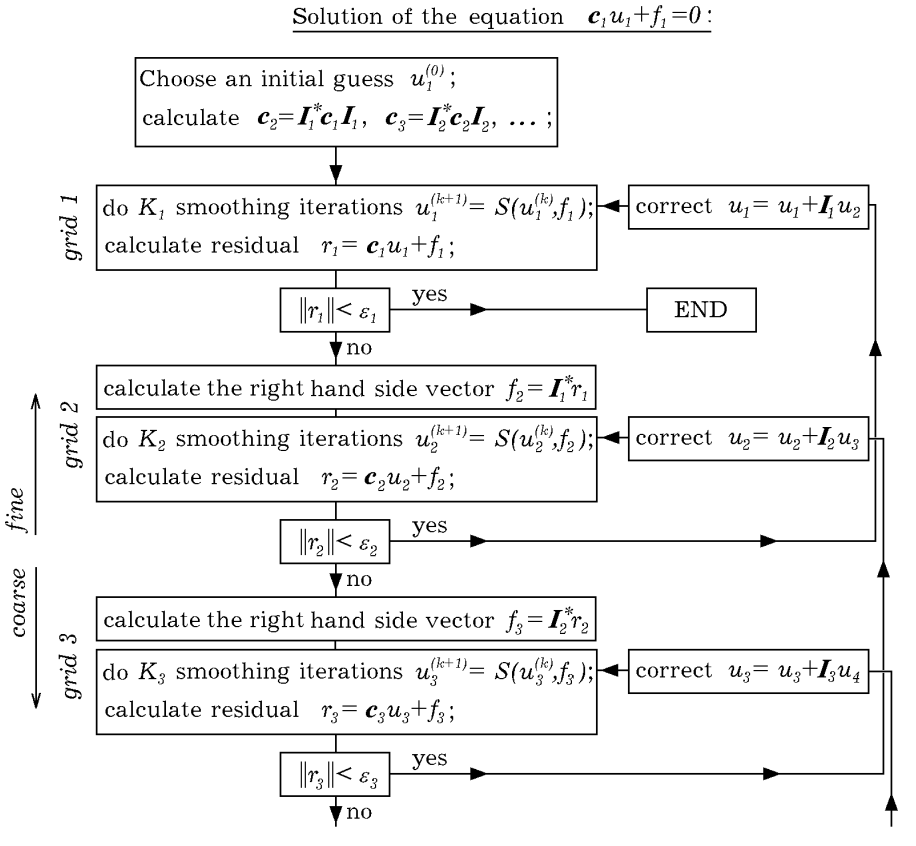

Figure 4.
General scheme of the multigrid algorithm

smoothing algorithm; $\boldsymbol{I}_l$ is an interpolation operator from a coarse grid of the level $l-1$ to a finer one of the level l, and $\boldsymbol{I}_l^*$ are the transpose operators. Subscripts indicate the number of grid levels starting from the finest one. Positive constants $\varepsilon_2, \varepsilon_3, \ldots$ define the accuracy requirements when solving the problems on coarse grids; $K_1, K_2, \ldots$ are the number of smoothing iterations that have to be done on corresponding grids. These parameters are pre-set by the user. We used $\varepsilon_l \approx 0.1, 0.2$, $l = 2, 3, \ldots$, and $K_l \approx 2, 4$, $l = 1, 2, \ldots$ and seven levels of grid. On the coarsest grid a direct method was employed to solve the corresponding algebraic equations.

The application of the multigrid method leads to a more complex scheduler than the commonly used "V-cycling" one. In this case the scheduler depends on the algebraic problem under consideration. As follows from the description of the method, a solution on a finer grid is:

- corrected using a solution on a coarser grid; and
- iterated up to the required accuracy.

The novelty of our approach is associated with a special way of formulating the algebraic problem on a coarse grid of the level $l-1$ when going from a previous finer grid of the level l to the coarser one. They are derived in such a way that when going backwards from the coarse grid of the level $l-1$ to the finer one of the level l, a correction of the pre-calculated solution u_l provides an exact weak solution on the finer grid of the level l. More specifically the transpose operators $\boldsymbol{I}_l^*$ are used to derive the matrices c_{l-1} and the right hand side vectors f_{l-1} as shown below.

Here we only consider an interaction between approximate solutions on two consequent grids. Let us denote the fine grid as f-grid and the coarse or rough grid as R-grid. Let subscript i denote a multi-index of dimension 2 and indicate a grid point everywhere below. We shall also use small letters to denote quantities on the f-grid and capital letters to denote quantities on the R-grid.

(1) Let us write a system of algebraic equations in the following general form

$$\sum_{\alpha=-1}^{1} c_i^{\alpha} u_{i+\alpha} + f_i = 0, \quad \mathbf{x} \in \omega_p. \tag{47}$$

In the general two-dimensional case the nine-point stencil is used, although some of the coefficients c_i^{α} can be equal to zero. There is no need to add boundary conditions to (47), as they are incorporated into this equation. In the general case, one can easily do this by eliminating the boundary equations and modifying c_i^{α} and f_i at adjacent internal points.

(2) Simple relaxation iterative methods (such as the point Jacobi iterations) are usually used as a smoother for the multigrid method. Let us consider the simplest one, namely, the point Jacobi iterations in the

one-dimensional case. At ith grid point it yields

$$u_i^{(k+1)} = u_i^{(k)} - \frac{1}{c_i^0} r_i^{(k)}, \quad \text{where} \quad r_i = \sum_{\alpha=-1}^{1} c_i^\alpha u_{i+\alpha} + f_i. \qquad (48)$$

Here r_i is the ith component of the residual, and k denotes the number of iteration. Performing this computation only at ith point, one obtains the following values of residual components at $i-1$th, ith and $i+1$th points

$$\tilde{r}_{i-1} = r_{i-1}^{(k)} - \frac{c_{i-1}^1}{c_i^0} r_i^{(k)}, \quad \tilde{r}_i = 0, \quad \tilde{r}_{i+1} = r_{i+1}^{(k)} - \frac{c_{i+1}^{-1}}{c_i^0} r_i^{(k)},$$

where $\tilde{r}$ are updated values of the residual. For the symmetric operator (i.e. $c_{i-1}^1 = c_i^{-1}$), and under condition $\sum_{\alpha=-1}^{1} c_i^\alpha = 0$ we have the following properties of (48):

- the computation of (48) at ith point does not change the sum $\sum_i r_i$ except at the points adjacent to the boundaries at which conditions different from the Neumann conditions are specified. Hence, for the Laplace operator this sum is changed only at the points adjacent to the boundaries with Dirichlet boundary conditions.
- if residual components $r_{i-1}^{(k)}, r_i^{(k)}, r_{i+1}^{(k)}$ have the same sign and the ith cell is not the boundary cell, then computation of (48) at the ith point does not change the residual norm $\|r\|_1 \equiv \sum_i |r_i|$.
- The residual norm can change (decrease) only in two cases: if the ith cell is on the boundary or the signs of $r_{i-1}^{(k)}, r_i^{(k)}$ and $r_{i+1}^{(k)}$ are not the same.

Hence, the Jacobi iterative method is efficient when $r_i^{(k)}$ is a highly oscillating function repeatedly changing its sign. For a function u with smooth residual r the method becomes inefficient.

Note that the same properties of residuals remain valid for more complex problems, including the following approximation of the Lame equations:

$$u_{x^-x^+} + u_{y^-y^+} + v_{xy}^{\circ\circ} + f_1 = 0,$$

$$v_{x^-x^+} + v_{y^-y^+} + u_{xy}^{\circ\circ} + f_2 = 0.$$

Here we used the notation u_{x^+}, u_{x^-} and u_x° for corresponding forward, backward and central differences defined by (5). In this case we do not have a diagonally dominant matrix (which is traditionally associated with the convergence of the process) but the Jacobi iterative method was successfully used as a "smoother" in the multigrid method by Fedorenko (1996). Note, however, that in our problem we use a different type of "smoother" that is the line relaxation iterative method with alternating

x_1 and x_2 directions. This is due to the inefficiency of the point relaxation method (48) when it is applied to an operator with the values of c_i^{α} in different directions being substantially different. Just this situation takes place in the problem in question when very different spatial steps are used for different directions near the prism.

(3) The next step in implementing the method is the construction of the R-grid. The R-grid is obtained by choosing the points of the f-grid with even components of multi-index i. Special treatment of the cells near the boundaries is needed. Finally, every point of the f-grid is placed inside or at the boundary of the corresponding R-grid cell. After that an interpolation operator $\boldsymbol{I}$, $\boldsymbol{I} : U \rightarrow u$, from the R-grid to the f-grid needs to be constructed. For every f-grid point, j, we find a rectangular $(J, J + A)$ containing this point. These points J of the R-grid are eventually used for interpolation of R-function into the point j. If the point j lies on the boundary of the rectangular $(J, J + A)$ then only the R-grid points from this boundary are used for the interpolation. Weights of interpolation are inversely proportional to distances from the f-grid points to the R-grid points. These distances are introduced as the Euclidean norms in the finite-dimensional space of f-grid points with index values for the coordinates of the points.

(4) The following idea is the basic one in the multigrid method. Suppose that a function u with a smooth residual is obtained after several iterations of (48) and further iterations change its value only negligibly. Let us obtain a correction function U on the R-grid (R-function). Let us try to obtain this function from the equation:

$$c(u + \boldsymbol{I}U) + f = 0. \tag{62}$$

This, however, turns out to be impossible as the number of unknown quantities U_i in (49) is less than the number of equations (the first number is equal to the number of R-grid points, and the second number is equal to the number of f-grid points).

Since we cannot solve (49), let us find its weak solution. For this purpose the so-called weak variational form of (49) can be stated as: find U such that

$$((\boldsymbol{c}(u + \boldsymbol{I}U) + f) \cdot \boldsymbol{I}V) = 0 \tag{50}$$

for every V. This approach is close to the one used in finite element methods where the weighted residual form of equations is used. In our case $\boldsymbol{I}V$ is used for the weighted (test) function.

Equation (50) can be rewritten in the following alternative form:

$$(\boldsymbol{I}^*(\boldsymbol{c}(u + \boldsymbol{I}U) + f) \cdot V) = 0, \quad \forall V,$$

where $\boldsymbol{I}^*$ is the transpose operator. This yields that

$$\boldsymbol{C}U + F = 0, \quad \text{where} \quad \boldsymbol{C} = \boldsymbol{I}^* \boldsymbol{c} \boldsymbol{I}, \quad F = \boldsymbol{I}^* r. \tag{51}$$

This is the required equation for the function U on the R-grid.

We can make the following important statement:

If U is the solution of (51) on the R-grid and $\tilde{u}$ the corrected approximate solution on the f-grid:

$$\tilde{u} = u + \boldsymbol{I}U$$

then the residual $\tilde{r} = \boldsymbol{c}\tilde{u} + f$ satisfies the equation:

$$(\tilde{r} \cdot \boldsymbol{I}V) = 0, \quad \forall V. \tag{52}$$

The proof is straightforward. To obtain it, one should substitute $\tilde{r}$ into (52) and take into account (50).

Taking the grid δ-function on the R-grid for V, we obtain the following important property of $\tilde{r}$. For a small number of f-grid points (just those that are involved in interpolation from one R-grid point), the sum of residual components $\tilde{r}_i$ with some positive weights is equal to zero. It means that $\tilde{r}_i$ often changes its sign and is a high-oscillating function. Hence, the relaxation iterations of (48) are again efficient after correction.

We conclude this section by making the following remarks.

Remark 1. Computation of the operator $\boldsymbol{C} = \boldsymbol{I}^* \boldsymbol{c} \boldsymbol{I}$ is computer expensive. For the problem under consideration, however, this operator does not depend on time, and needs to be calculated only once at the beginning of computation. In the general case this operator may be calculated for several time steps if it is weakly dependent on time. This can be justified since (51) is solved with a low accuracy (the criterion $\|R\| \leq \varepsilon \|F\|$ is used in the calculations with $\varepsilon \approx 0.1 - 0.2$).

Remark 2. The phenomenon of stencil spreading (i.e. a process of involving more grid points into an equation) occurs. It means that the operator $C = I^* \boldsymbol{c} \boldsymbol{I}$ has a nine-point stencil (for two-dimensional problems) in all cases, even if the operator c has a one-point stencil. However, there is no further spreading of the stencil beyond nine points.

5. Results

All results were obtained for the dimensionless geometry parameters $d = 1$, $L = 60, H = 24, l = 6$ and $V_\infty = 1$ (see Figure 1) and the main flow parameters are introduced as follows. The Strouhal number Str is defined by fd/V_∞, where f is a vortex-shedding frequency. C_D and C_L, the drag and lift coefficients, are defined by $F_D/(\frac{1}{2}\rho V_\infty^2 d)$ and $F_L/(\frac{1}{2}\rho V_\infty^2 d)$ respectively, where F_D and F_L are the drag and lift forces. C_{Lrms} denotes the root-mean-square lift coefficient defined as $(\overline{C_L^2})^{\frac{1}{2}}$.

Non-uniform computational grids were used with the local grid Reynolds number Re_h near the prism surfaces ranged from 0.6 to 2 for different Reynolds

numbers. The grid Reynolds number Re_h is defined by $\mathrm{Re}\,h/d$, where h is the dimensionless spatial grid step. Spatial grid steps near the prism were $h_{min} = 0.01$ for $\mathrm{Re} = 100$, 200, and in the range from $h_{min} = 0.01$ to $h_{min} = 0.0012$ for $\mathrm{Re} = 500$. These cases were iterated until periodic states were achieved. The latter were determined by monitoring the variations of local flow parameters and the drag and lift coefficients for some (usually five) periods. Within each time step the integral norm (analogue of the norm in L_2) of the continuity equation residual was less than the dimensionless value of 10^{-6}.

The dimensionless time step was chosen small enough ($\tau = 0.02$) in order to obtain time-step independent results when using a method of the first-order accuracy in time.

In the calculations the uniform flow parameters were used as initial conditions. First, symmetric flow was observed, then it became unstable, lost symmetry and transformed into a periodic flow. Unstable modes are introduced into the solution via numerical errors.

Figures 5, 6, 8 and 9 show streak lines of the numerically simulated flow for several values of Re and at different time moments. These will be described in the following subsections.

5.1 Von Karman streets at Re = 100 and 200

Figures 5 and 6 show the calculated streak lines around a square prism and in the wake for Re = 100 and 200. Impressive von Karman vortex streets, which are very regular at these Reynolds numbers, are clearly seen in these Figures.

Time histories of C_D, C_L and other integral parameters show a periodic structure with a dominant harmonic at these Reynolds numbers. Each cycle involves the shedding of a pair of eddies from the prism. The drag coefficient oscillates at twice the frequency of the lift coefficient, as the drag is not sensitive to the asymmetry of the shedding. The time-averaged drag coefficients ($\overline{C}_D$), the Strouhal numbers (Str) and other characteristics of the flows are presented in Table II.

Figure 7 shows a comparison between the values of the time-averaged drag coefficient $\overline{C}_D$ and the Strouhal number Str calculated in our paper and

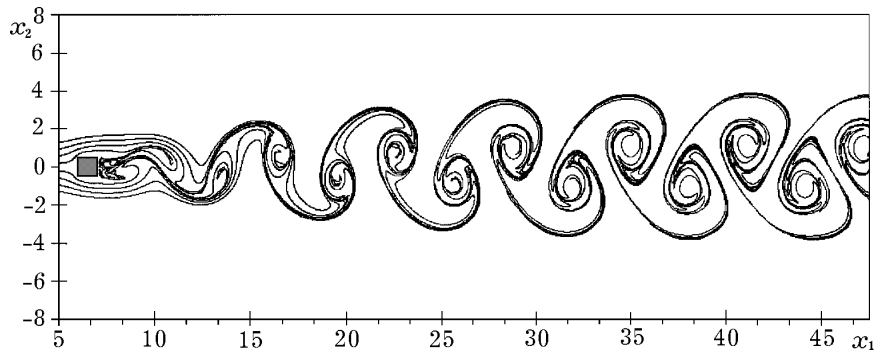

Figure 5.
The flow around a square prism and in the wake at Re = 100

previously obtained experimental and numerical results. As can be seen, the calculated Strouhal number and drag coefficient are close to those reported by other authors, especially to the recent paper by Sohankar *et al.* (1998).

5.2 Flow at Re = 500

Starting from a uniform flow in the whole domain at $t = 0$, after $t = 30T$, where T is the period of the leading harmonic, a highly periodic flow was obtained for Re = 500. Variations of the velocity at the point lying on the centre line, at 0.25d behind the prism were less than 0.01 per cent over five periods.

The integral characteristics of the flow are presented in Table II. The stagnation pressure coefficient C_{ps} is defined by $(p_s - p_\infty)/(\frac{1}{2}\rho V_\infty^2)$, and the base pressure coefficient C_{pb} is defined by $(p_b - p_\infty)/(\frac{1}{2}\rho V_\infty^2)$, where p_s and p_b are pressure values at the central points of forward and backward faces of the prism.

Str_1, Str_2 and Str_3 indicate Strouhal numbers corresponding to the first three harmonics as indicated in Figure 10. To ensure that grid-independent results are obtained, calculations were performed at sequentially halved time steps, $\tau = 0.04$, 0.02 and 0.01, and on a sequence of spatial grids with 201×161 and 401×321 grid points with $h_{min} = 0.01$, 0.005, 0.0025 and 0.00125. On

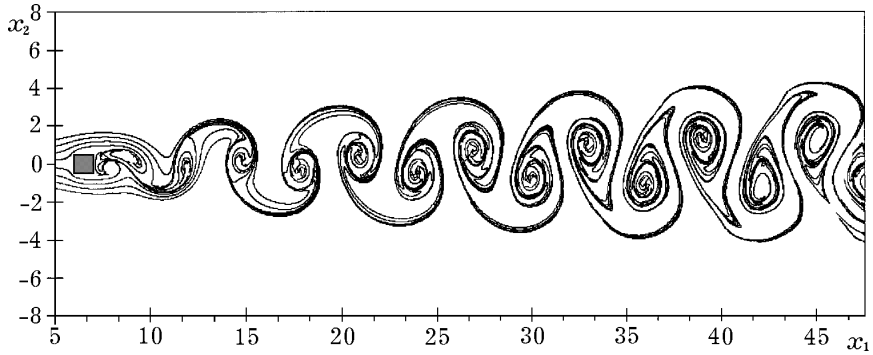

Figure 6.
The flow around a square prism and in the wake at Re = 200

Re	Grid	Str	$\overline{C}_D$	C_{Lrms}	$\overline{C}_{ps}$	$-\overline{C}_{pb}$
100	400×320 ($h_{min} = 0.01$	0.150	1.51	0.137	1.14	0.678
200	400×320 ($h_{min} = 0.01$	0.156	1.56	0.376	1.11	0.859
500	200×160 ($h_{min} = 5 \times 10^{-3}$)	$Str_1 = 0.096$ $Str_2 = 0.175$ $Str_3 = 0.271$	2.31	1.32	1.07	1.65
	400×320 ($h_{min} = 2.5 \times 10^{-3}$)	$Str_1 = 0.088$ $Str_2 = 0.176$ $Str_3 = 0.264$	2.23	1.20	1.09	1.56
	400×320 ($h_{min} = 1.25 \times 10^{-3}$)	$Str_1 = 0.0876$ $Str_2 = 0.175$ $Str_3 = 0.263$	2.22	1.18	1.12	1.50

Table II.
Calculated parameters of the flow around the square prism

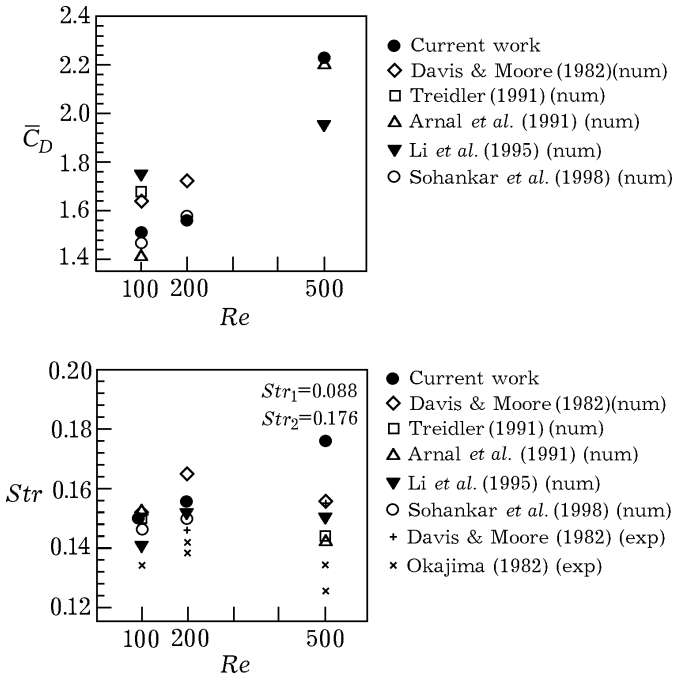

Figure 7.
A comparison between time-averaged drag coefficient $\overline{C}_D$ and Strouhal number Str reported by various authors (numerical (num) and experimental (exp) results) and obtained from our computations

decreasing τ from 0.02 to 0.01, values of C_D and Str changed by less than 1 per cent. This value of $\tau = 0.02$ is proved to be suitable to obtain results within 1-2 per cent of their τ-independent values (Arnal *et al.*, 1991; Li and Humphrey, 1995; Sohankar *et al.*, 1998).

Figure 8 shows detailed views of the flow near the prism for eight successive moments of time, which span over the whole period. These instants are indicated in Figure 10 in order to link the flow patterns with the time history of the drag coefficient. The streak lines and lines of constant pressure (isobars) shown in this Figure allow us to see details of the flow around the prism. Four vortices were shed during the period shown in Figure 8. Two of these vortices are the von Karman vortices, which were formed just behind the prism. Two other vortices appear on the top and bottom surfaces of the prism. Shedding of these vortices strongly influences the shedding of the von Karman vortices and the flow in the wake. The formation of these lateral vortices is itself influenced by the motion of the von Karman vortices.

Comparing the streak lines shown in Figure 8 with the time history of the drag coefficient shown in Figure 10, one can see that the shedding of each eddy leads to a sudden drop in the drag. The number of local minima of the drag coefficient shown in Figure 10 is equal to the number of shed eddies.

In Figure 9 the streak lines are shown for the wake behind the prism for the same moments of time as in Figure 8. The interaction of eddies with opposite signs and different intensities can be seen. The interaction of eddies with the same sign is also observed in the vicinity of the centre line, albeit not as clearly.

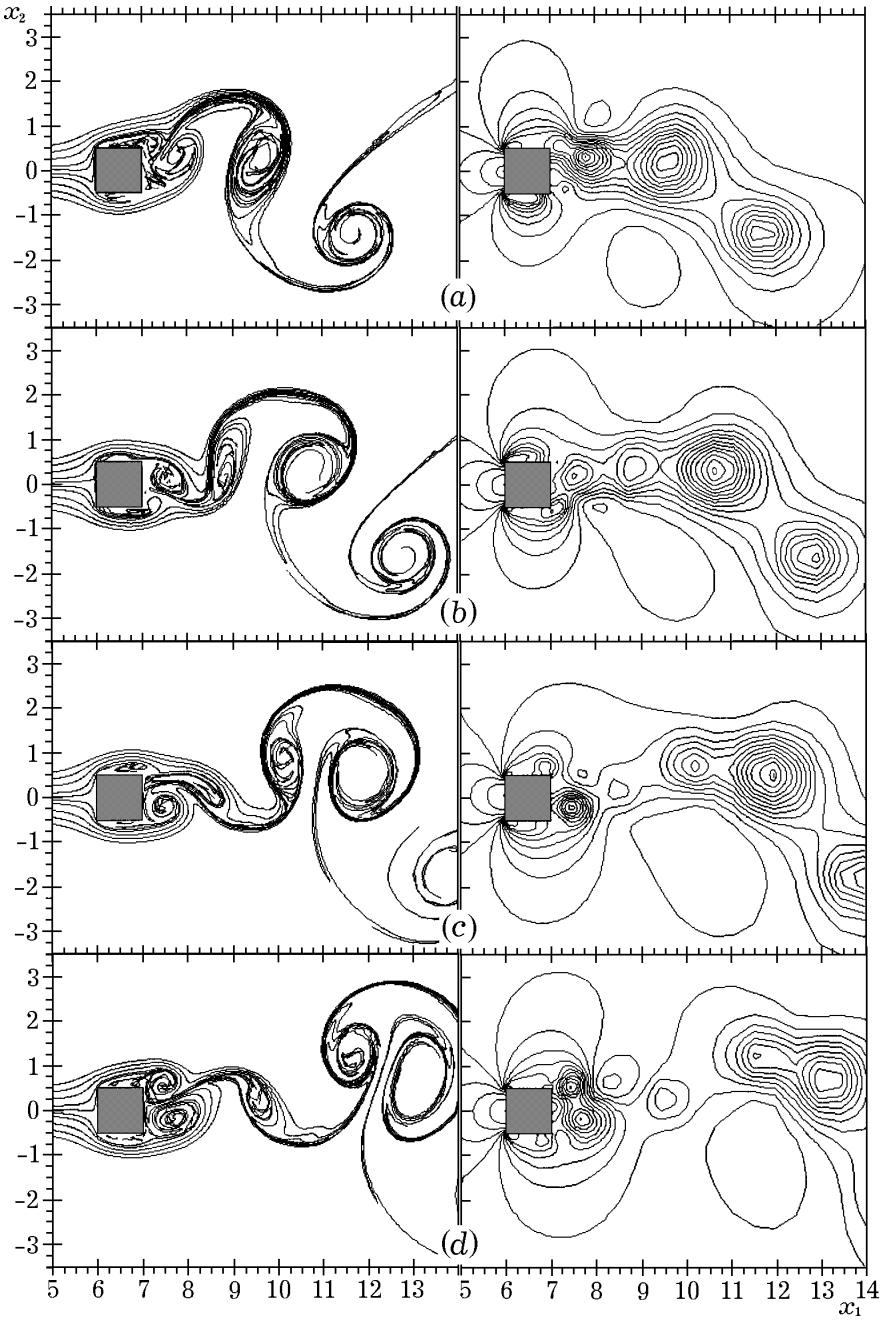

Figure 8.
Streak lines and lines of constant pressure (isobars) in the vicinity of the square prism for Re = 500 at the moments of time:
(a) $t = t_0$;
(b) $t = t_0 + T/8$;
(c) $t = t_0 + 2T/8$;
(d) $t = t_0 + 3T/8$
(e) $t = t_0 + 4T/8$;
(f) $t = t_0 + 5T/8$;
(g) $t = t_0 + 6T/8$;
(h) $t = t_0 + 7T/8$

(*Continued*)

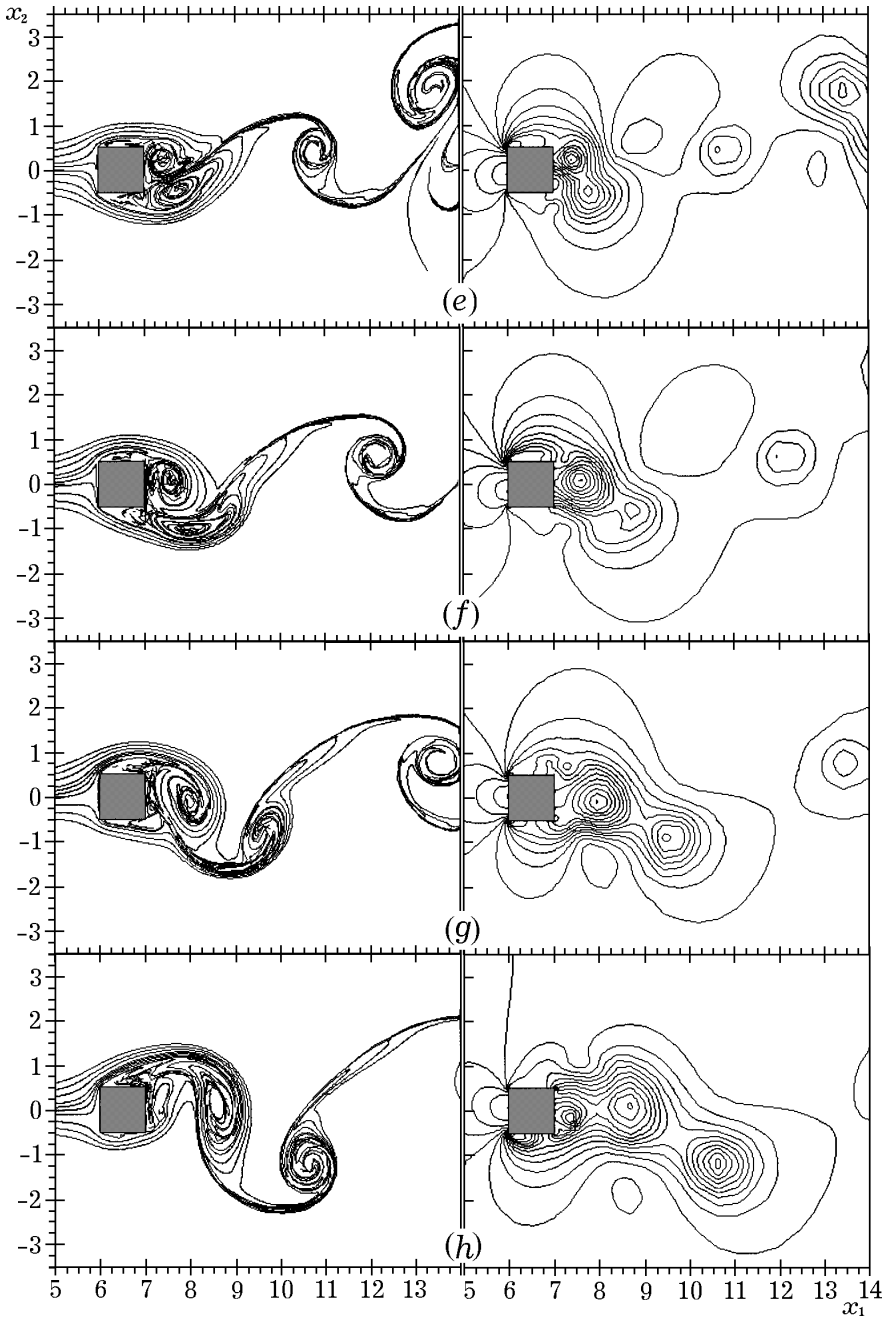

Figure 8.

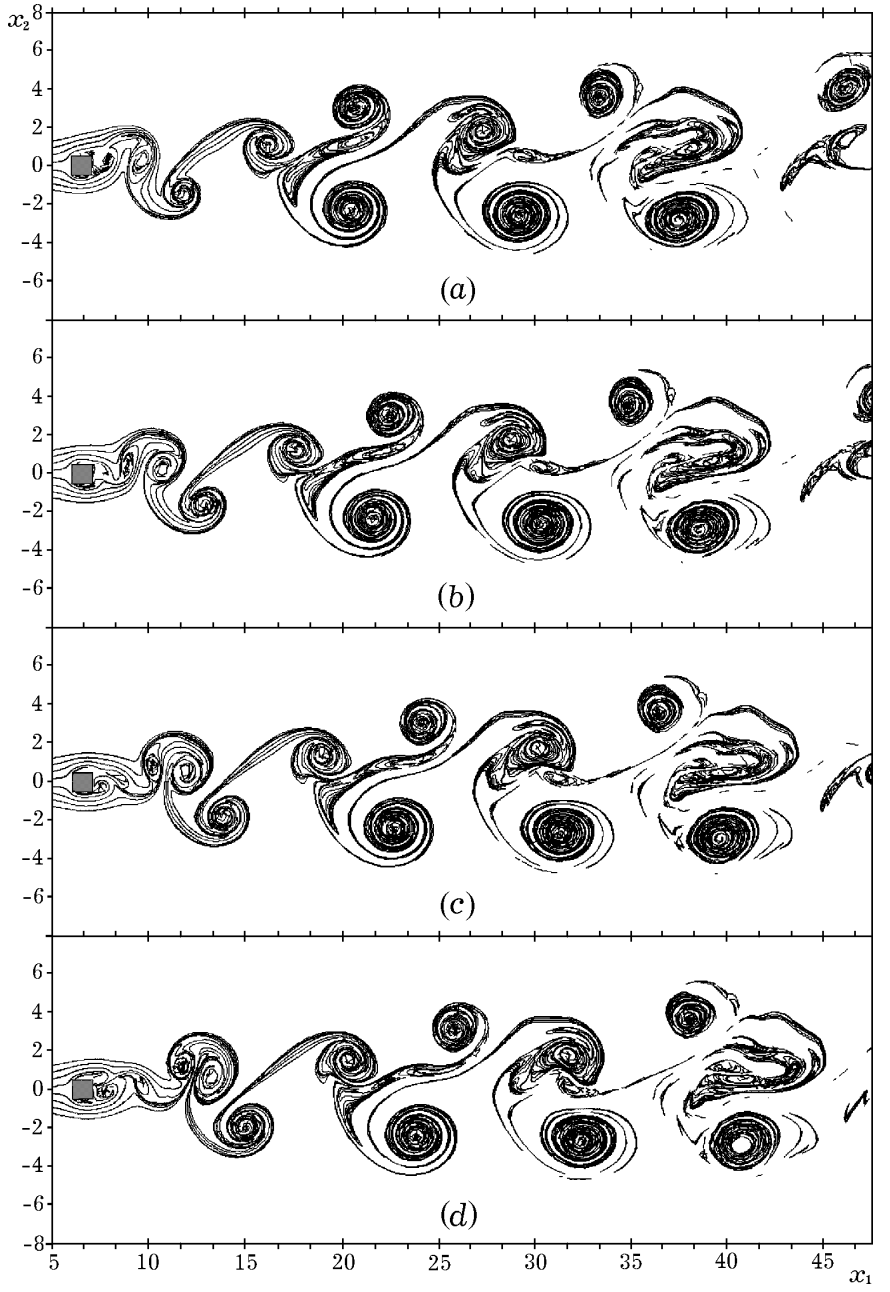

Figure 9.
Streak lines in the wake area for Re = 500 at the moments of time:
(a) $t = t_0$;
(b) $t = t_0 + T/8$;
(c) $t = t_0 + 2T/8$;
(d) $t = t_0 + 3T/8$
(e) $t = t_0 + 4T/8$;
(f) $t = t_0 + 5T/8$;
(g) $t = t_0 + 6T/8$;
(h) $t = t_0 + 7T/8$

(*Continued*)

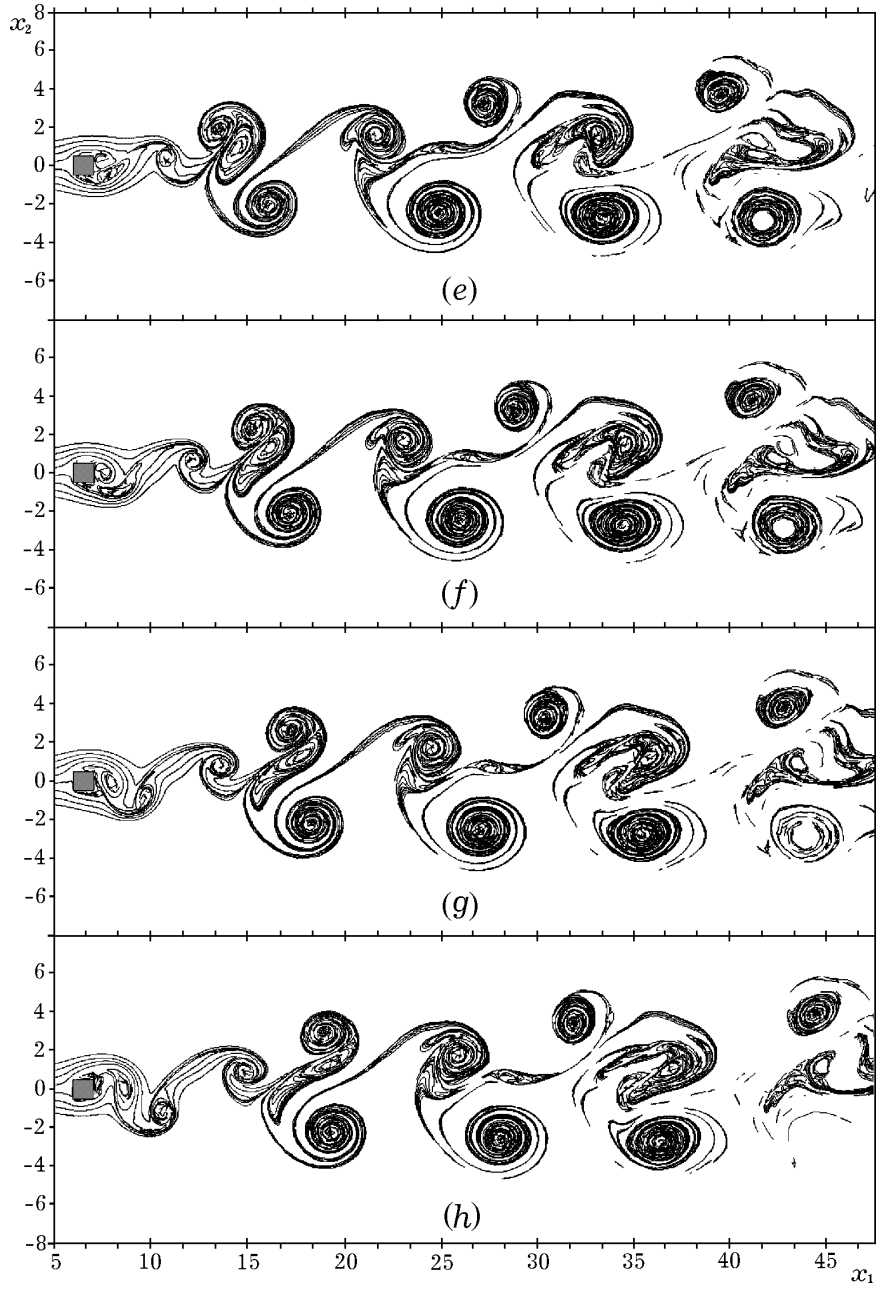
x_2
8
6
4
2
0
-2
-4
-6
(e)
6
4
2
0
-2
-4
-6
(f)
6
4
2
0
-2
-4
-6
(g)
6
4
2
0
-2
-4
-6
-8
(h)
5
10
15
20
25
30
35
40
45
x_1

Figure 9.

As already mentioned, Figure 10 shows the time history of the drag and lift coefficients (C_D and C_L) and their spectral analysis. The presence of several harmonics in the spectra of the drag and lift coefficients reflects the complex nature of the flow at these values of Re. The leading harmonic in the lift coefficient corresponds to Str $\approx$ 0.18 which is close to the ones calculated from empirical formulae. For example, the formula presented by Douglas *et al.* (1995) gives:

$$\mathrm{Str} = 0.198\left(1 - \frac{19.7}{\mathrm{Re}}\right)$$

Although this formula was originally obtained for a circular cylinder it can be used for approximate estimates of Str for bodies of other shapes, including a square prism. It is applicable in the range $250 < \mathrm{Re} < 2 \times 10^5$. For Re = 500 it predicts Str = 0.19 which agrees with our results.

The complex spectral structure of the flow around a square prism is not a new result. Similar observations have been made by several authors (e.g. Okajima, 1982). The novelty of our contribution is in the observation of a striking difference in the spectral structures of the drag and lift coefficients. The dominant frequency of the drag coefficient is found to be equal to about half the dominant frequency of the lift coefficient. For Re = 500 the spectral structures of the drag and lift coefficients and the correlation between them differ from those at Re = 100 and 200. The reason for this can be inferred from the correlation between flow pictures shown in Figure 8 and properties of the drag and lift coefficients shown in Figure 10. As to the drag coefficient, it is mainly controlled by the shedding and merging of two main vortices, while the shedding of two small vortices does not seem to have a significant influence on this process. Hence, the drag coefficient has only one sharply pronounced maximum for a period. In contrast to this, the lift coefficient strongly depends on the growth and shedding of every vortex, and has two maxima and two

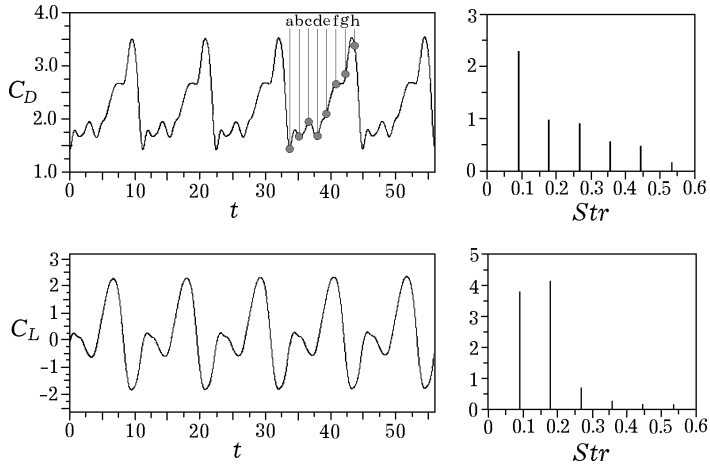

Figure 10.
Time history of the drag coefficient C_D and the lift coefficient C_L, and the results of their spectral analysis for Re = 500. Points in the C_D versus time plot correspond to the moments of time at which the plots in Figures 8(a-h) and 9(a-h) are shown

minima in its period. The average value of the drag coefficient and the Strouhal numbers corresponding to the leading harmonics for Re = 500 are shown in Figure 7. As can be seen from this Figure, the predicted value of the drag coefficient is close to the one reported earlier by Arnal *et al.* (1991). At the same time the predicted value of the Strouhal number is slightly higher than the one predicted by other authors and observed experimentally. We cannot provide a rigorous explanation of the reasons for this small difference in the predicted values of Str, but we can draw readers' attention to the fact that the experimental setup used both by Okajima (1982) and Davis *et al.* (1984) refers to a confined three-dimensional flow rather than to the free two-dimensional flow which we modelled. The same remark refers to the numerical results reported by Davis *et al.* (1984) and Li and Humphrey(1995). In both cases confined flows were calculated.

It is reasonable that the drag coefficient for a square prism appears to be higher than the drag coefficient for a circular cylinder for which this coefficient is close to 1 (cf. Figure 14.14 of Panton, 1996). This indicates that the square prism is naturally a more significant obstacle for the flow when compared with a circular cylinder.

As can be seen from Figures 8 and 9, the flow is not symmetrical about the centre line. This suggests the existence of another unsteady flow, which is mirror symmetric to the one shown in these Figures. In order to obtain this second flow we used the mirror transformed pressure and velocity fields of the calculated flow as initial conditions for new calculations. Figure 11(a-c) shows three flows at Re = 500. The first one, presented in Figure 11(a), is an unstable steady flow, which was obtained when the symmetry condition was imposed at the centre line. Figure 11(b) shows the earlier described periodic flow, and Figure 11(c) shows the second periodic flow around the prism which is mirror symmetric to that in Figure 11(b) with respect to the centre line. Several periods were calculated for this second transient flow to ensure that this is a stable flow mirror symmetric with respect to the first.

When a prediction is started with symmetric initial conditions, a particular structure of numerical errors of the method defines which of two observed flows will be reproduced in a calculation. We sometimes observed switching flow after a fully periodic flow was randomly perturbed. No other flows were obtained in our calculations but we cannot guarantee that there are no other transient flows around the square prism at Re = 500.

Comparing our results with the ones obtained by Arnal *et al.* (1991), we can see that in our case we obtained a fully periodic flow while Arnal *et al.* (1991) reported a non-periodic flow (e.g. see their Figures 2 and 7). We can attribute this to the finer spatial grids used in our calculations. When we used coarser grids, we also obtained a non-periodic flow similar to the one reported by Arnal *et al.* (1991). The time-averaged values of the drag coefficient and their time histories are close to those reported by Arnal *et al.* (1991). The time history of the lift coefficient, however, is different from those reported by Arnal *et al.* (1991). Also the values of the base shedding frequency obtained in our paper

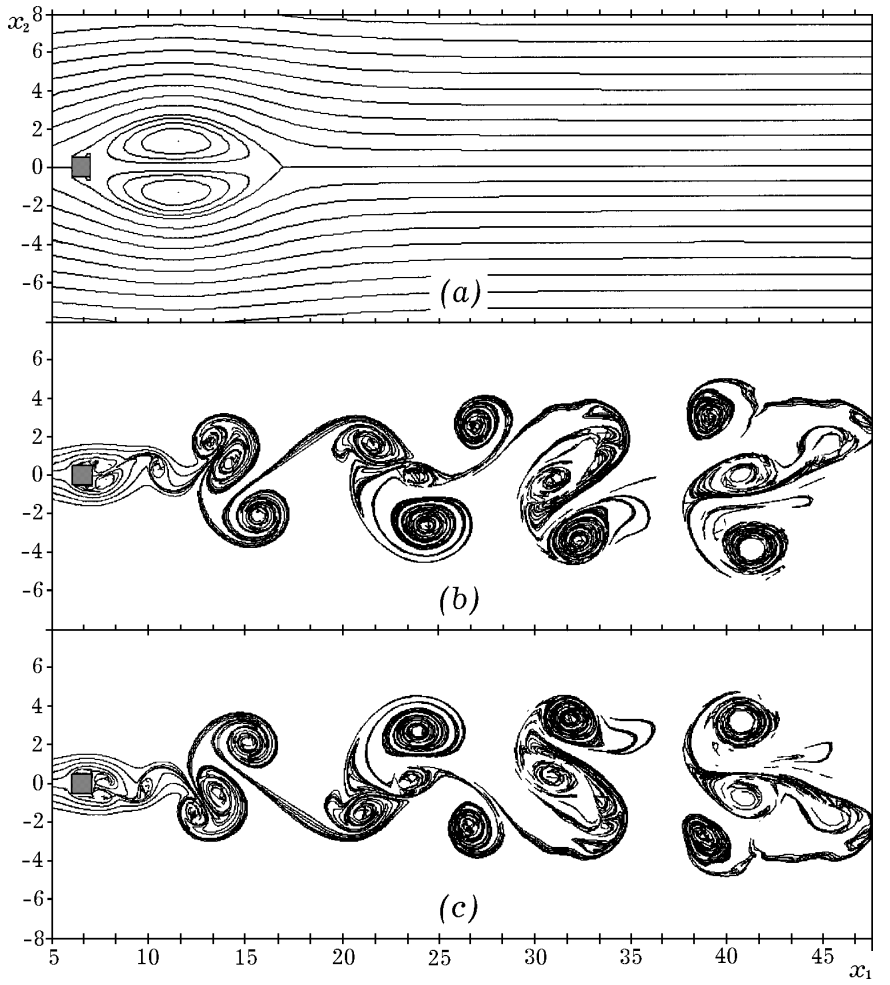

Figure 11.
Three flows around a square prism at Re = 500: (a) symmetrical (unstable) steady flow; (b) and (c) unsteady, mirror symmetric flows

and by Arnal *et al.* (1991) are slightly different as well. Note that the value of $C_{Lrms} = 1.35$ predicted by Arnal *et al.* (1991) is close to the one calculated in this paper ($C_{Lrms} = 1.20$).

An interesting feature of the obtained results is that the time-averaged lift coefficient is not exactly equal to zero due to the non-symmetry of the flow. Although the accuracy of the calculations of this parameter is not sufficient even for $h_{min} = 0.0012$, its precise non-zero value can be obtained with confidence on finer grids.

To demonstrate the robustness of this method that uses the central differences for convective terms, we have solved the problem at $\mathrm{Re} = 5 \cdot 10^5$. We used the same grid with 401×321 grid points and $h_{min} = 0.0012$, and the same time step $\tau = 0.02$. Figure 12 shows detailed views of the flow near the prism and in the wake behind the prism for a time moment; the predicted flow is fairly smooth; the drag coefficient is $C_D = 1.37$. Of course the solution suffers

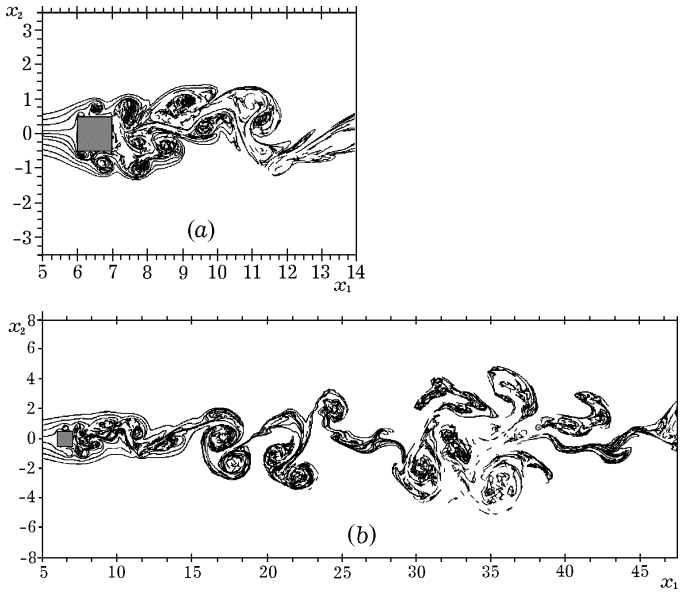

Figure 12.
Streak lines: (a) in the vicinity; and (b) in the wake area of the square prism for Re = $5 \cdot 10^5$

from scheme dissipation in this case. Solution of the pressure equation by the multigrid takes the same computational time, and the computational time for solving the non-symmetric momentum equations by preconditioned ORTHOMIN(1) (Saad, 1996) is about two times longer than the time required to solve the flow at Re $\leq$ 500.

6. Comparison of the multigrid and iterative methods

To demonstrate the efficiency of the modified multigrid method, it was compared with one of the well-known iterative methods, namely, the modified incomplete Cholesky factorisation-conjugate gradient method (Saad, 1996) (ICCG). An efficient implementation of the method (that employs the so-called Eisenstat trick) was kindly provided by Makarov (Kutcherov and Makarov, 1984) for the comparison. Figure 13 shows the results of this comparison.

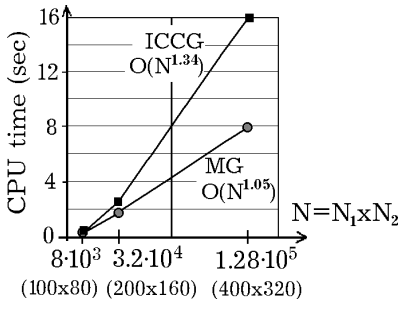

Figure 13.
A comparison of the multigrid method (MG) and the modified incomplete Cholesky factorisation – conjugate gradient method (ICCG). CPU time required to solve the pressure problem for a given time step versus the number of grid points

Average CPU times for solving the pressure equation per time step are presented for the sequence of spatial grids. As can be seen, the multigrid method is more than two times faster on the grid 401×321 and has a more promising asymptotic rate when compared with the iterative method. The asymptotic rate for the multigrid method is found to be about $O(N)$ which could not be achieved by any other method.

7. Conclusions

Results of numerical calculations of the unsteady, two-dimensional incompressible flow around a square prism and in the near wake at $\mathrm{Re} = 100$, 200 and 500 are presented. An implicit finite-difference operator-splitting (SIMPLEC-like) method on a staggered grid to solve the continuity and Navier-Stokes equations is described and implemented. This method has second-order accuracy in space, and conserves mass, momentum and kinetic energy. The robustness of the method is illustrated by solving the problem at $\mathrm{Re} = 5 \cdot 10^5$ without noticeable increase of CPU time. A modified multigrid method is described and employed to solve the elliptic pressure problem. New features that improve the efficiency of this approach are explored. The modified multigrid method is compared with a single-grid iterative method and is found to be more efficient especially for a large number of cells. The CPU time required by this method is shown to be approximately proportional to the number of cells to the power 1.05. Calculations have been performed on a sequence of spatial grids with up to 401×321 grid points and at sequentially halved time steps to ensure that grid-independent results (within 2 per cent) are obtained.

It is shown that three flows exist at $\mathrm{Re} = 500$. The first is a steady-state unstable flow and the other two are transient, periodic, asymmetric about the central line, and are mirror symmetric to each other. The asymmetric flows can generate a non-zero lift coefficient, and these are the only flows which can be observed in practice. The steady-state symmetrical flow does not reproduce adequately the physical nature of the flow. In contrast to some previous results these flows are shown to be fully periodic, but the spectral structures of the drag and lift coefficients are shown to be noticeably different. The leading harmonic of the lift coefficient corresponds to $\mathrm{Str} \approx 0.18$ for $\mathrm{Re} = 500$. The previously reported non-periodic nature of the flow was reproduced when a coarser grid was used for the computations.

The method of flow calculation presented in this paper enables the accurate and effective prediction of the flow which can be applied to various engineering problems as an alternative to available commercial CFD packages. It is particularly important for the prediction of flow in compact heat exchangers where heat transfer enhancement is achieved by the introduction of discrete wall roughness and/or vortex generators. The application of this method would allow engineers to study the effect of different parameters quickly and efficiently leading to the optimum design of these heat exchangers.

References

Anderson, D.A. (1995), *Computational Fluid Dynamics*, McGraw-Hill.

Arakawa, A. (1966), "Computational design for long-term numerical integration of the equations of fluid motion: two-dimensional incompressible flow. Part 1", *J. Comput. Phys.*, Vol. 1, pp. 119-43.

Arnal, M.P., Goering, D.J. and Humphrey, J.A.C. (1991), "Vortex shedding from a bluff body on a sliding wall", *J.Fluids Eng.*, Vol. 113, pp. 384-98.

Belotzerkovskii, S.M., Kotovskii, V.N., Nisht, M.I. and Fedorov, R.M. (1988), *Mathematical Modelling of Two-Dimensional Flows with Separations*, Nauka, Moscow, (in Russian).

Blevins, R.D. (1977), *Flow Induced Vibrations*, Van Nostrand Reinhold Company.

Botta, E.F.F., Dekker, K., Notay, Y., van der Ploeg, A., Vuik, C., Wubs, F.W. and de Zeeuw, P.M. (1997), "How fast the Laplace equation was solved in 1995", *Appl. Numer. Math.*, Vol. 24, pp. 439-55.

Churbanov, A.G., Pavlov, A.N. and Vabishchevich, P.N. (1995), "Operator-splitting methods for the incompressible Navier-Stokes equations on non-staggered grids. Part 1: First-order schemes", *Int. J. Numer. Methods Fluids*, Vol. 21, pp. 617-40.

Coleman, H.W. and Stern, F. (1998), "Uncertainties and CFD code validation", *J. Fluid Engineering*, Vol. 119, pp. 795-803.

Davis, R.W. and Moore, E.F. (1982), "A numerical study of vortex shedding from rectangles", *J. Fluid Mech.*, Vol. 116, pp. 474-506.

Davis, R.W., Moore, E.F. and Purtell, L.P. (1984), "A numerical-experimental study of confined flow around rectangular cylinders", *Phys. Fluids*, Vol. 27, pp. 46-59.

Douglas, J.F., Gasioret, J.M. and Swaffield, J.A. (1995), *Fluid Mechanics*, Longman, Harlow.

Douglass, R.W. and Ramshaw, J.D. (1994), "Perspective: future research directions in computational fluid dynamics", *Transactions of the ASME*, Vol. 116, pp. 212-15.

Durgin, W.W. and Karlsson, S.K.F. (1971), "On the phenomenon of vortex breakdown", *J. Fluid Mechanics*, Vol. 48, pp. 507-27.

Fedorenko, R.P. (1964), "The speed of convergence of one iterative process", *USSR Comp. Math. and Math. Phys.*, Vol. 4, pp. 227-35.

Fedorenko, R.P. (1973), "Iterative solution of difference elliptic equations", in Russian, *Uspekhi Matematicheskikh Nauk (Advances in Mathematical Sciences)*, Vol. 28, pp. 123-82.

Fedorenko, R.P. (1996), "Finite super-elements method and multigrid method in problems of elasticity theory", *Comp. Fluid Dynamics J.*, Vol. 5, pp. 203-12.

Fiebig, M. (1995), "Vortex generation for compact heat exchangers", *J. Enhanced Heat Transfer*, Vol. 2, pp. 43-61.

Fletcher, C.A.J. (1997), *Computational Techniques for Fluid Dynamics*, Springer.

Franke, R., Rodi, W. and Schonung, B. (1990), "Numerical calculation of laminar vortex-shedding flow past cylinders", *J. Wind Eng. Ind. Aerodyn.*, Vol. 35, pp. 237-57.

Fryazinov, I.V. and Moiseenko, B.D. (1981), "Conservative finite difference schemes for incompressible viscous flows using Euler variables", *Zhurnal vichislitelnoy matematiki i matematicheskoy fiziki (Journal of Computational Mathematics and Mathematical Physics)*, (in Russian), Vol. 21 No. 5, pp. 1180-91.

Fryazinov, I.V., Mazhorova, O.S. and Marchenko, M.P. (1994), "Monotone corrective terms and coupled algorithm for the Navier-Stokes equations of an incompressible flow", *Matematicheskoe Modelirovanie (Mathematical Modeling)*, (in Russian), Vol. 6 No. 12, pp. 97-116.

Hackbusch, W. (1994), *Iterative Solution of Large Systems of Equations*, Springer-Verlag, New York, NY.

Henk, A. and van der Vorst, (1981), "Iterative solution methods for certain sparse linear systems with a non-symmetric matrix erasing from PDE-problems", *J. Comput. Phys.*, Vol. 44, pp. 60-78.

Hojo, K., Matsushima, E. and Sakakura, H. (1997), "On open boundary conditions for two-dimensional incompressible flow problem", in Zhuang, F.G. (Ed.), *Proceedings of the 7th International Symposium on Computational Fluid Dynamics*, 15-19 September, Beijing, China, pp. 274-9.

Igarashi, T. (1984), "Characteristics of the flow around a square prism", *Bull. JSME*, Vol. 27, pp. 1858-65.

Igarashi, T. (1985), "Heat transfer from a square prism to an air stream", *Int. J. Heat Mass Transfer*, Vol. 28, pp. 175-81.

Karniadakis, G.E. and Triantafyllou, G.S. (1992), "Three-dimensional dynamics and transition to turbulence in the wake of bluff objects", *J. Fluid Mech.*, Vol. 238, pp. 1-30.

Kondo, N. and Yamada, S. (1995), "Third-order upwind finite element computation of the incompressible Navier-Stokes equations. Part I. Computation of flow around rectangular cylinders", *Comput. Methods Appl. Mech. Engrg*, Vol. 127, pp. 87-97.

Kutcherov, A.B. and Makarov, M.M. (1984), "An approximate factorization method for solving finite-difference elliptic problems with mixed boundary conditions", *Vichislitelnie metodi matematicheskoy fisiki (Numerical Methods in Mathematical Physics)*, (in Russian), Moscow State University, Moscow, pp. 54-65.

Ladysenskaya, O.A. (1969), *The Mathematical Theory of Viscous Incompressible Flows*, Gordon and Breach, New York, NY.

Leonard, A. (1980), "Vortex methods for flow simulation", *J. Computational Physics*, Vol. 37, pp. 289-335.

Leonard, B.P. (1979), "A stable and accurate convective modeling procedure based on quadratic upstream interpolation", *Comput. Methods Appl. Mech. Eng.*, Vol. 19, pp. 59-98.

Li, G. and Humphrey, J.A.C. (1995), "Numerical modelling of confined flow past a cylinder of square cross-section at various orientations", *Int. J. Numer. Methods Fluids*, Vol. 20, pp. 1215-36.

Marchuk, G.I. (1982), *Methods of Numerical Mathematics*, Springer-Verlag, Berlin.

Nagano, S., Naito, M. and Takata, H. (1982), "A numerical analysis of two-dimensional flow past a rectangular prism by a discrete vortex model", *J. Fluid Mech.*, Vol. 116, pp. 474-506.

Okajima, A. (1982), "Strouhal numbers of rectangular cylinders", *J. Fluid Mech.*, Vol. 123, pp. 379-98.

Okajima, A. (1990), "Numerical simulation of flow around rectangular cylinders", *J. Wind Eng. Ind. Aerodyn.*, Vol. 33, pp. 171-80.

Okajima, A., Ueno, H. and Sakai, H. (1992), "Numerical simulation of laminar and turbulent flows around rectangular cylinders", *Int. J. Numer. Methods Fluids*, Vol. 15. pp. 999-1012.

Panton, R.L. (1996), *Incompressible Flow*, John Wiley & Sons.

Patankar, S.V. (1980), *Numerical Heat Transfer and Fluid Flow*, McGraw-Hill.

Ramos, J.I. (1989), *Internal Combustion Engine Modelling*, Hemisphere Publishing Corporation.

Rhie, C.M. and Chow, W.L. (1983), "Numerical study of the turbulent flow past an airfoil with trailing edge separation", *AIAA Journal*, Vol. 21, pp. 1525-32.

Roache, P.J. (1997), "Quantification of uncertainty in computational fluid dynamics", *Annu. Rev. Fluid Mechanics*, Vol. 29, pp. 123-60.

Saad, Y. (1996), *Iterative Methods for Sparse Linear Systems*, PWS Publishing Company, Boston, MA.

Saffman, P.G. (1995), *Vortex Dynamics*, Cambridge University Press.

Samarskii, A.A. (1989), *Theory of Difference Schemes*, (in Russian), Nauka, Moscow.

Sarpkaya, T. (1989), "Computational methods with vortices", *J. Fluid Engineering*, Vol. 111, pp. 5-52.

Sarpkaya, T. (1994), "Vortex element method for flow simulation", *Adv. Appl. Mech.*, Vol 31, pp. 113-247.

Sarpkaya, T. (1996), "Vorticity, free surface, and surfactants", *Annu. Rev. Fluid Mechanics*, Vol. 28, pp. 83-128.

Sazhin, S.S., Wild, P., Sazhina, E.M., Makhlouf, M., Leys, C. and Toebaert, D. (1994), "Three-dimensional modelling of processes in the fast-axial-flow CO_2 laser", *J Physics D: Applied Physics*, Vol. 27, pp. 464-9.

Schumm, M., Berger, E. and Monkewitz, P.A. (1994), "Self-excited oscillations in the wake of 2-D bluff bodies and their control", *J. Fluid Mechanics*, Vol. 271, pp. 17-53.

Shih, T.M., Tan, C.H. and Hwang, B.C. (1989), "Effects of grid staggering on numerical schemes", *Int. J. Numer. Methods Fluids*, Vol. 9 No. 2, pp. 193-212.

Sohankar, A., Norberg, C. and Davidson, L. (1998), "Low-Reynolds-number flow around a square cylinder at incidence: study of blockage, onset of vortex shedding and outlet boundary condition", *Int. J. Numer. Methods Fluids*, Vol. 26, pp. 39-56.

Tafti, D. (1996), "Comparison of some upwind-based high-order formulations with a second-order central-difference scheme for time integration of the incompressible Navier-Stokes equations", *Computers & Fluids*, Vol. 25, pp. 647-65.

Tamura, T. (1990a), "Numerical study of aerodynamic behavior of square cylinders", *J. Wind Eng. Ind. Aerodyn.*, Vol. 33, pp. 161-70.

Tamura, T. (1990b), "On the reliability of two-dimensional simulation for unsteady flows around a cylinder-type structure", *J. Wind Eng. Ind. Aerodyn.*, Vol. 35, pp. 275-98.

Treidler, E.B. (1991), "An experimental and numerical investigation of flow past ribs in a channel", PhD thesis, University of California at Berkeley, CA.

Vabishchevich, P.N., Pavlov, A.N. and Churbanov, A.G. (1996), "Numerical methods for unsteady incompressible flows using primitive variables and non-staggered grids", *Matematicheskoe Modelirovanie (Mathematical Modeling)* in Russian, Vol. 8 No. 7, pp. 81-108.

Vabishchevich, P.N., Pavlov, A.N. and Churbanov, A.G. (1997), "Numerical methods for the unsteady Navier-Stokes equations using primitive variables and partially staggered grids", *Matematicheskoe Modelirovanie (Mathematical Modeling)* in Russian, Vol. 9 No. 4, pp. 85-114.

Veldman, A.E.P. (1990), "'Missing' boundary conditions? Discretize first, substitute next, and combine later", *SIAM J. Sci. Stat. Comput.*, Vol. 11 No. 1, pp. 82-91.

Webb, R.L. (1994), *Principles of Enhanced Heat Transfer*, John Wiley & Sons.

Wesseling, P. (1991), *An Introduction to Multigrid Methods*, John Wiley & Sons.

Williamson, C.H.K. (1988), "The existence of two stages in the transition to three-dimensionality of a cylinder wake", *Phys. Fluids*, Vol. 31, pp. 3165-8.

Williamson, C.H.K. (1996), "Vortex dynamics in the cylinder wake", *Ann. Rev. Fluid Mech.*, Vol. 28, pp. 477-539.

Wissink, J.G. (1995), "DNS of transitional flow around a square cylinder", *Advances in Turbulence V*, Kluwer, Dordrecht, pp. 569-73.

Wissink, J.G. (1997), "DNS of 2D turbulent flow around a square cylinder", *Int. J. Numer. Methods Fluids*, Vol. 25, pp. 51-62.

Xi, G.N., Hagiwara, Y. and Suzuki, K. (1995), "Flow instability and augmented heat transfer of fin arrays", *J. Enhanced Heat Transfer*, Vol. 2, pp. 23-32.

Zhang, L.W., Tafti, D.K., Najjar, F.M. and Balachandar, S. (1997), "Computations of flow and heat transfer in parallel-plate fin heat exchangers on the CM-5: effects of flow unsteadiness and three-dimensionality", *Int. J. Heat Mass Transfer*, Vol. 40, pp. 1325–41.

Appendix A. Properties of discrete operators

Here we prove properties (40)-(42) of operators div_h, grad_h, $\mathsf{C}_h(\mathbf{v})$ and D_h defined in Section 4.2. We use interpolated velocities $\dot{v}_i$ and $\hat{v}_i$, $i = 1, 2$, and notation $(v_i)_{x_j^+}$, $(v_i)_{x_j^-}$ and $(v_i)^\circ_{xj}$ for the corresponding forward, backward and central differences as they are introduced in Section 4.1.

I. Let us prove that

$$(\mathrm{grad}_h p \cdot \mathbf{w}) = 0 \tag{A1}$$

for any $\mathbf{w} \in \mathcal{H}^2_{sol}$. The proof follows from the sequence of equations:

$$(\mathrm{grad}_h p \cdot \mathbf{w}) = \sum_{\mathbf{x}\in\omega_{v_1}} \frac{p_{i+1,j} - p_{i,j}}{h_1}\, w_{1i,j}\, h_1 h_2 + \sum_{\mathbf{x}\in\omega_{v_2}} \frac{p_{i,j+1} - p_{i,j}}{h_2}\, w_{2i,j}\, h_1 h_2$$

$$= -\sum_{\mathbf{x}\in\omega_p} \left(p_{i,j} \frac{w_{1i,j} - w_{1i-1,j}}{h_1} + p_{i,j} \frac{w_{2i,j} - w_{2i,j-1}}{h_2} \right) h_1 h_2 = -\sum_{\mathbf{x}\in\omega_p} p\, \mathrm{div}_h \mathbf{w}\, h_1 h_2 = 0,$$

where we used the condition $\mathrm{div}_h \mathbf{w} = 0$, $\mathbf{x} \in \omega_p$.

II. Let us show that

$$(\mathsf{C}_h(\mathbf{w})\mathbf{v} \cdot \mathbf{v}) = 0 \tag{A2}$$

for any $\mathbf{w} \in \mathcal{H}^2_{sol}$ and $\mathbf{v} \in \mathcal{H}^2$ with zero values at boundary.

At first we write

$$\left((\dot{w}_1 \dot{v}_1)_{x_1^+} \cdot v_1 \right)_{v1} = \sum_{i=1}^{N_1-1} \sum_{j=1}^{N_2} \frac{1}{4h_1} \Big((w_{1i+1,j} + w_{1i,j})(v_{1i+1,j} + v_{1i,j})$$

$$- (w_{1i,j} + w_{1i-1,j})(v_{1i,j} + v_{1i-1,j}) \Big) v_{1i,j} h_1 h_2$$

$$= \sum_{i=1}^{N_1-1} \sum_{j=1}^{N_2} \frac{1}{4h_1} \Big((w_{1i+1,j} - w_{1i-1,j}) v_{1i,j}^2 + (w_{1i+1,j} v_{1i+1,j} - w_{1i-1,j} v_{1i-1,j}) v_{1i,j}$$

$$+ (v_{1i+1,j} + v_{1i-1,j}) w_{1i,j} v_{1i,j} \Big) h_1 h_2 = \sum_{i=1}^{N_1-1} \sum_{j=1}^{N_2} \frac{1}{4h_1} (w_{1i+1,j} - w_{1i-1,j}) v_{1i,j}^2 h_1 h_2$$

$$= \left((w_1)^\circ_{x_1} \cdot v_1^2 \right)_{v1}.$$

Therefore, we have

$$\left((\dot{w}_1 \dot{v}_1)_{x_1^+} \cdot v_1 \right)_{v1} = \left((w_1)^\circ_{x_1} \cdot v_1^2 \right)_{v1}. \tag{A3}$$

Next we obtain

$$\left((\hat{w}_2\hat{v}_1)_{x_2^-}\cdot v_1\right)_{v1}=\sum_{i=1}^{N_1-1}\sum_{j=1}^{N_2}(\hat{w}_2\hat{v}_1)_{x_2^-}v_1\,h_1h_2=-\sum_{i=1}^{N_1-1}\sum_{j=0}^{N_2-1}\hat{w}_2\hat{v}_1(v_1)_{x_2^+}\,h_1h_2$$

$$=-\sum_{i=1}^{N_1-1}\sum_{j=0}^{N_2-1}\tfrac{1}{2}\hat{w}_2(v_1^2)_{x_2^+}\,h_1h_2=\sum_{i=1}^{N_1-1}\sum_{j=1}^{N_2}\tfrac{1}{2}(\hat{w}_2)_{x_2^+}v_1^2\,h_1h_2$$

$$=\sum_{i=1}^{N_1}\sum_{j=1}^{N_2}\tfrac{1}{4}(w_2)_{x_2^-}(v_{1i-1,j}^2+v_{1i,j}^2)\,h_1h_2$$

Using the continuity equation $(w_1)_{x_1^-}+(w_2)_{x_2^-}=0$ to replace $(w_2)_{x_2^-}$ by $-(w_1)_{x_1^-}$, we can continue the sequence of equations

$$=-\sum_{i=1}^{N_1}\sum_{j=1}^{N_2}\tfrac{1}{4}(w_1)_{x_1^-}(v_{1i-1,j}^2+v_{1i,j}^2)\,h_1h_2=\sum_{i=1}^{N_1-1}\sum_{j=1}^{N_2}\frac{1}{4h_1}(v_{1i+1,j}^2-v_{1i-1,j}^2)w_{1i,j}\,h_1h_2$$

$$=\left(\tfrac{1}{2}(v_1^2)_{\circ_{x_1}}\cdot w_1\right)_{v1}.$$

Hence, we get

$$\left((\hat{w}_2\hat{v}_1)_{x_2^-}\cdot v_1\right)_{v1}=\left(\tfrac{1}{2}(v_1^2)_{\circ_{x_1}}\cdot w_1\right)_{v1}. \tag{A4}$$

Combining (A3) and (A4) we obtain

$$\left(\left((\dot{w}_1\dot{v}_1)_{x_1^+}+(\hat{w}_2\hat{v}_1)_{x_2^-}\right)\cdot v_1\right)_{v1}=\left((w_1)_{\circ_{x_1}}\cdot v_1^2\right)_{v1}+\left((v_1^2)_{\circ_{x_1}}\cdot w_1\right)_{v1}=0. \tag{A5}$$

In a similar way we obtain

$$\left(\left((\hat{w}_1\hat{v}_2)_{x_1^-}+(\dot{w}_2\dot{v}_2)_{x_2^+}\right)\cdot v_2\right)_{v2}=0. \tag{A6}$$

Now (A2) directly follows from (A5) and (A6).

III. Let us show that

$$(\mathbf{D}_h\mathbf{v}\cdot\mathbf{v})\geq 0 \tag{A7}$$

for any $\mathbf{v}\in\mathcal{H}^2$ with zero Dirichlet or Neumann conditions at boundary.

We start with the relation

$$\left(-\mathbf{D}_{x_1}^{v_2}v_2\cdot v_2\right)_{v2}=-\sum_{i=1}^{N_1}\sum_{j=1}^{N_2-1}\left(\mathbf{D}_{x_1}^{v_2}v_2\right)_{i,j}v_{2i,j}\,h_1h_2 \tag{A8}$$

and consider the term

$$-\sum_{i=1}^{N_1}\left(\mathbf{D}_{x_1}^{v_2}v_2\right)_{i,j}v_{2i,j}\,h_1 \tag{A9}$$

at any fixed j. Let x_1-line passes through the prism at this j (see Figure 3). To simplify manipulations, denote $v_{2i,j}$ by y_i. Now we have

$$-\sum_{i=1}^{N_1}\left(D_{x_1}^{v_2}y\right)_i y_i\, h_1 = \frac{1}{h_1}\Big(y_1(y_1-y_0)+(y_2-y_1)^2+\cdots$$

$$+\underbrace{(y_{i_L}-y_{i_L-1})^2+3y_{i_L}^2-\tfrac{1}{3}y_{i_L}^2y_{i_L-1}^2}_{A}+\underbrace{3y_{i_R}^2-\tfrac{1}{3}y_{i_R}^2y_{i_R+1}^2+(y_{i_R+1}-y_{i_R})^2}_{B}+\cdots$$

$$+(y_{N_1}-y_{N_1-1})^2+(y_{N_1}-y_{N_1+1})y_{N_1}\Big)$$

As one can see, the first and the last members of the sum are greater than zero at zero Dirichlet conditions $y_0 = 0$, $y_{N_1} = 0$, and are equal to zero at zero Neumann conditions $y_1 - y_0 = 0$, $y_{N_1} - y_{N_1+1} = 0$. For terms A and B, it is also easy to show that they are greater than zero for any non-zero values of y_i. Therefore (A8) and consequently (A9) are greater than zero for any $y \neq 0$ and equal zero for $y = 0$.

In a similar way we obtain that $-D_{x_1}^{v_1} \geq 0$, $-D_{x_2}^{v_1} \geq 0$ and $-D_{x_2}^{v_2} \geq 0$. Hence inequality (A7) holds true.

Appendix B. Use of non-uniform grid

In order to ensure the validity of (40)-(42) for the discrete operators div_h, grad_h, $C_h(\mathbf{v})$ and D_h in the case of non-uniform grid, one should define the interpolated velocities $\hat{v}_1$ and $\hat{v}_2$ by slightly modified expressions (see Figure A1):

$$\hat{v}_{1i,j} = \frac{h_{2j}}{h_{2j+1}+h_{2j}}v_{1i,jj} + \frac{h_{2j+1}}{h_{2j+1}+h_{2j}}v_{1i,jj+1},$$

$$\hat{v}_{2i,jj} = \frac{h_{1i}}{h_{1i+1}+h_{1i}}v_{2i,jj} + \frac{h_{1i+1}}{h_{1i+1}+h_{1i}}v_{2i+1,jj},$$

$$i = 0,1,,N_1, j = 0,1,,N_2.$$

Interpolated velocities $\dot{v}_1$, $\dot{v}_2$ remain the same. The scalar products are defined using local space steps. For example,

$$(u\cdot w)_{v_1} = \sum_{\mathbf{x}\in\omega_{v_1}} u(\mathbf{x})w(\mathbf{x})\tfrac{1}{2}(h_{1i}+h_{1i+1})\,h_{2j}, u, w \in \mathcal{H}_{v_1}.$$

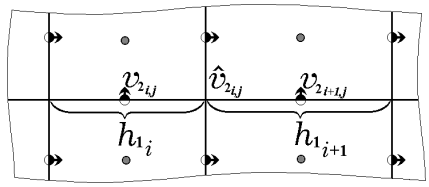

Figure A1.
Interpolated velocity components on non-uniform grid